Leukemia-associated Nup214-fusion proteins disturb XPO1-mediated nuclear-cytoplasmic transport pathway and thereby NF-κB signaling pathway

Shoko Saito[a, b]#, Sadik Cigdem [a]*, Mitsuru Okuwaki[a, b], Kyosuke Nagata[c]

Graduate School of Comprehensive Human Sciences[a], and Department of Infection Biology, Faculty of Medicine, University of Tsukuba, Tsukuba, Japan[b]; University of Tsukuba, Tsukuba, Japan[c]

Running Head: SET/DEK-Nup214 disturbs export and transcription

#Address correspondence to Shoko Saito, ssaito@md.tsukuba.ac.jp

*Present address: Sadik Cigdem, Turgut Özal University Medical Faculty, Ankara, Turkey.

S.S. and S.C. contributed equally to this work.

The word count for the Materials and Methods: 703 words

The combined word count for the Introduction, Results, and Discussion: 4030 words

Abstract

Nuclear-cytoplasmic transport though nuclear pore complexes is mediated by nuclear transport receptors. Previous reports suggested that aberrant nuclear-cytoplasmic transport by mutations or overexpression of nuclear pore complexes and nuclear transport receptors is closely linked to diseases. Nup214, a component of nuclear pore complexes, has been found as chimeric fusion proteins in leukemia. Among various Nup214-fusion proteins, SET-Nup214 and DEK-Nup214 were shown to be engaged in tumorigenesis, but their oncogenic mechanism remains unclear. In this study, we examined the function of the Nup214-fusion proteins by focusing on their effects on nuclear-cytoplasmic transport. We found that SET-Nup214 and DEK-Nup214 interact with XPO1/CRM1 and NXF1/TAP, which mediate leucine-rich NES-dependent protein export and mRNA export, respectively. SET-Nup214 and DEK-Nup214 decreased XPO1-mediated nuclear export of NES proteins such as cyclin B and proteins involved in the NF-κB signaling pathway by tethering XPO1 onto nuclear dots where Nup214-fusion proteins are localized. We also demonstrated that SET-Nup214 and DEK-Nup214 expression inhibited NF-κB-mediated transcription by abnormal tethering of the complex containing p65 and its inhibitor, IκB, in the nucleus. These results implicate that SET-Nup214 and DEK-Nup214 perturb gene expression regulation through alteration of the nuclear-cytoplasmic transport system.

Introduction

Biological macromolecules are transported between the nucleus and the cytoplasm in response to extracellular signals. Transport of molecules with a molecular mass greater than 40 kDa does not occur by simple diffusion, but is generally facilitated by nuclear transport receptors (NTRs) through nuclear pore complexes (NPCs) embedded in the nuclear envelope (1-3). Controlled nuclear-cytoplasmic transport plays important roles in maintaining cellular integrity in eukaryotic cells. It is reported that aberrant subcellular localization of some proteins is associated with various cancer cases (4). p53 has nuclear localization signal (NLS) and nuclear export signal (NES), and the accumulation of p53 in the cytoplasm has been reported to be a prognostic indicator in cancer (5). Nuclear factor-kappa B (NF-κB) transcription factor is mainly observed in the cytoplasm in normal cells, whereas in many cancer cells it is largely localized in the nucleus (6).

In addition to aberrant subcellular localization of proteins in cancer, mutations of genes encoding NTRs and NPC components are found in various types of cancer (7). Mutations of Exportin-5 (XPO5) and Exportin-1 (XPO1)/CRM1, members of export receptors, (8-10) are found in solid cancer and leukemia, respectively. Four nucleoporins, Nup98, Nup214/CAN, Nup358/RanBP2, and Tpr, have been reported to form chimeric proteins by chromosomal translocations mainly in leukemia (11-15). Nup214 located at the cytoplasmic filament of NPC interacts with NTRs to control macromolecular transport. *Set-nup214* and *dek-nup214* were identified in acute undifferentiated leukemia and acute myeloid leukemia (AML), respectively (16, 17), and recently found in several T cell acute lymphoid leukemia (T-ALL) and AML

patients (18, 19). SET-Nup214 is found to bind to the *hoxa* locus and activate its expression (20). Ectopic expression of SET-Nup214 causes expansion of hematopoietic progenitors (21, 22), and blocks cell differentiation (23). Expression of DEK-Nup214 leads to acceleration of protein synthesis (24), cell proliferation (25), and development of leukemia in mice (26). However, the detailed functions of these fusion proteins in leukemogenesis remain unclear.

Nup214 interacts with various NTRs such as Importin-β (IPOB)(27, 28), Exportin-T (XPOT)(29), XPO1(30), Nuclear RNA export factor 1 (NXF1)/TAP (31-34), NXF2, and NXF3 (35). Export of both mRNAs and proteins is severely reduced when the level of Nup214 expression is decreased (36-38), and ectopic overexpression of truncated Nup214 causes accumulation of NES proteins in the nucleus in mammals (39). On the other hand, in *Drosophila*, *nup214* deletion enhances export of GFP fused with NES (40). These results indicate that appropriate expression of Nup214 is critical for regulated export of macromolecules and that generation of fusion genes containing Nup214 by chromosomal translocation may affect the nuclear-cytoplasmic transport system (41).

In previous studies, we and another group reported that both SET-Nup214 and DEK-Nup214 interact with XPO1. This interaction causes a change in XPO1 localization and consequently impairs correct localization of an artificial model protein containing NES (28, 42, 43). Here, we comprehensively analyzed the effects of SET-Nup214 and DEK-Nup214 expression on the functions of NTRs and their cargoes. We found that SET-Nup214 and DEK-Nup214 interact with NXF1 and XPO1, and abrogates the XPO1 function to dampen nuclear export of endogenous NES proteins such as cyclin B and proteins involved in the NF-κB pathway. In

addition, we demonstrated that SET-Nup214 and DEK-Nup214 expression inhibited NF-κB-mediated transcription due to abnormal retention of complexes containing p65 and its inhibitor, I kappa B (IκB), in the nucleus. These results suggest the possibility that perturbation of proper nuclear-cytoplasmic shutting of macromolecules by the expression of the Nup214-fusion proteins lead to various hematologic disorders.

Materials and Methods

Cell culture and transfection

HeLa cells and HEK293T cells were grown in DMEM supplemented with 10% fetal bovine serum and penicillin-streptomycin. For transfection assays, GeneJuice (Merck KGaA, Germany) (IF assay, luc assay, FRAP assay) or Polyethylenimine, Linear (MW 25,000) (Polysciences, Inc.) (IP assay, ChIP assay) was used.

Plasmids

For construction of NTR expression vectors, cDNAs were prepared from total RNA derived from HeLa and HEK293T cells by revers-transcription with ReverTra Ace (TOYOBO Co., Ltd, Japan) and oligo dT_{20}. PCR amplification was performed using KOD FX (TOYOBO Co., Ltd). PCR fragments were inserted into pCHA (44). pCAGGS-HA-XPO1 was made by inserting HA-tagged XPO1 fragment obtained by PCR using pXHC1 as a template into pCAGGS. pCAGGS-SET-Nup214-3Flag and pCAGGS-DEK-Nup214-3Flag were made by inserting amplified PCR fragment (C terminal fragment of Nup214 fused with three Flag-tags) using pCAGGS-SET-Nup214 as a template, into pCAGGS-SET-Nup214 or pCAGGS-DEK-Nup214. For pCAGGS-3Flag-Nup214 (1057-2090) and pCAGGS-3Flag-SET-Nup214 (1637), Nup214 (1057-2090) and SET-Nup214 (1637) was digested from pCAGGS-Nup214 (1057-2090) and pCAGGS-SET-Nup214 (1637), and inserted into pCAGGS-3Flag. pmKate2-C-SET-Nup214 and pmKate2-C-DEK-Nup214 were constructed by excising pmKate2-C (Evrogen) and ligated with SET-Nup214 and DEK-Nup214 excised from pCAGGS-SET-Nup214

and pCAGGS-DEK-Nup214. pEGFP-C1-NXF1 was constructed by ligation of a fragment excised from pEGFP-C1 (Clontech Laboratories, Inc.) with NXF1 fragment generated by PCR using pCHA-NXF1 as a template. To construct pNF-κB40-firefly luciferase, Interferon Stimulated Response Element (ISRE) of pISRE-TA-luc (Clontech Laboratories, Inc.) was removed, and a fragment of NF-κB binding element from pNF-κB-SEAP (Clontech Laboratories, Inc.) was inserted. To construct pTA-Renilla luciferase, ISRE of pISRE-TA-luc vector was removed, and the firefly luciferase region was replaced with a fragment of the Renilla luciferase region, which was obtained from pRL-SV40 (Promega). Sequences of all fragments obtained by PCR were confirmed by sequencing analysis.

Immunoprecipitation (IP) assay and western blot analysis

IP assays and western blot analyses were performed as described previously (45). To detect chemiluminescence in western blot analysis, Chemi-Lumi One L (Nacalai tesque, Inc., Japan) or ImmunoStar LD (Wako Pure Chemical Industries, Ltd., Japan) was used, and signals were observed using LAS-4000mini (GE Healthcare UK Ltd.), and processed by Adobe Photoshop Elements (Adobe Systems).

Immunofluorescence (IF) assay, oligo dT-mediated *in situ* hybridization, and Proximity Ligation Assay (PLA)

IF assays were performed as described previously (45). For DNA staining, TO-PRO-3 Iodide (Life Technologies) (1:5000) was used. For IF assays of spleen sections, sample sections with 2 μm in thickness were examined.

144 Paraffin-embedded sections were deparaffinized and rehydrated in xylene and ethanol.
145 Samples were autocleaved for 5 min in 10 mM citrate buffer solution. After washing
146 with PBS(-), samples were subjected to IF assays. *In situ* hybridization using oligo
147 dT was performed according to the protocol as described previously (46). PLA was
148 performed using Duolink In Situ PLA (Sigma-Aldrich Co. LLC) according to the
149 manufacturer's instructions after incubation with primary antibodies. After PLA,
150 samples were incubated with Alexa 488-conjugated anti-mouse IgG and Alexa
151 633-conjugated anti-rabbit IgG antibodies for 30 min to observe IκBα and p65,
152 respectively. Samples were observed by LSM5Exciter confocal microscope with
153 Plan-Apochromat 63x objective lens (Carl Zeiss Microscopy GmbH, Germany).
154 Pictures were processed by ZEN software (Carl Zeiss Microimaging GmbH,
155 Germany). Statistical analyses were performed by Student's t-test.

156

157 **RNA extraction and RT-qPCR**

158 Total RNA was extracted using MagExtractor -RNA- (TOYOBO Co., Ltd). The
159 experimental procedure was as described in the manufacturer's protocol. Total RNA
160 (0.5 μg) was reverse-transcribed by ReverTra Ace (TOYOBO Co., Ltd) and oligo
161 dT_{20} for 60 min at 42°C. For qPCR, Fast SYBR Green Master (Roche Diagnostics
162 GmbH) was mixed with reverse-transcribed samples and primers, and PCR was
163 carried out by Thermal Cycler Dice Real Time System (TAKARA BIO Inc. Japan).
164 Primer sequences used in this study were as follows: for A20, 5'-AAG CTG TGA
165 AGA TAC GGG AGA-3' and 5'-CGATGAGGGCTTTGTGGATGAT-3', for
166 IκBα/NFKBIA, 5'-CTCCGAGACTTTCGAGGAAATAC-3' and

5’-GCCATTGTAGTTGGTAGCCTTCA-3’, and for GAPDH, 5’-AGCCAAAAGGGTCATCATCTC-3’ and 5’-GGACTGTGGTCATGAGTCCTTC-3’. Statistical analyses were performed by Student’s t-test.

ChIP assay

ChIP assays were carried out according to the manual supplemented from Merck except for sonication buffer used in figure 7D. Sonication buffer; 640 mM KCl, 30 mM NaCl, 1% Triton X-100, 10 mM EDTA, 20mM Tris-HCl (7.9), and 20% glycerol. qPCR analysis was performed as described for RT-qPCR. Primer sequences used in this study were as follows: for A20, 5’-CAGCCCGACCCAGAGAGTCAC-3’ and 5’-CGGGCTCCAAGCTCGCTT-3’, and for IκBα/NFKBIA, 5’-ATTCAAATCGATCGTGGGAAAC-3’ and 5’-GGGAATTTCCAAGCCAGTCA-3’.

Results

SET-Nup214 and DEK-Nup214 interact with nuclear transport receptors

Nucleoporins can be categorized into three groups; transmembrane nucleoporins, scaffold nucleoporins, and nucleoporins containing phenylalanine-glycine repeats (FG-Nups). Nup214 is one of FG-Nups and interacts with several NTRs through its FG repeat region. Because both SET-Nup214 and DEK-Nup214 contain the intact FG repeat region of Nup214 (Figure 1A), it is possible that these fusion proteins interact with NTRs. Indeed, SET-Nup214 and DEK-Nup214 were shown to interact with XPO1 (42, 43). To verify whether SET-Nup214 and DEK-Nup214 bind to several NTRs other than XPO1, we first performed immunoprecipitation (IP) assays. We assessed seven well-known NTRs as follows; Importin-β1 (IPOB) (import of NLS-containing proteins), Importin-7 (IPO7) (import of proteins such as histone and MAPK), XPO1 (export of NES-containing proteins, snRNAs, and snoRNAs), Exportin-2 (XPO2) /CSE1L (export of Importin α), Exportin-5 (XPO5) (export of small RNAs), Exportin-3 (XPO3) /Exportin-t (export of tRNAs), and NXF1 (export of mRNAs). Among these NTRs, XPO1 and NXF1 bind to SET-Nup214 and DEK-Nup214 efficiently (Figure 1B). Because SET-Nup214 and DEK-Nup214 have a shared Nup214 portion (813-2090 a.a.) which is composed of coiled-coil and FG repeat domains, we addressed whether the binding of SET-Nup214 and DEK-Nup214 with NTRs was mediated by the Nup214 portion. The C-terminally truncated Nup214 (1057-2090) efficiently bound to XPO1 and NXF1 (Figure 1B), demonstrating the interaction between SET-Nup214 or DEK-Nup214 and XPO1 or NXF1 depends on the Nup214 part. Reciprocal IP experiments confirmed the interaction between SET-Nup214, DEK-Nup214, or Nup214 (1057-2090) and

207 endogenous XPO1 or NXF1 (Figure 1C).

208

209 **SET-Nup214 and DEK-Nup214 affect subcellular localization of nuclear**
210 **transport receptors**

211 As we and another group reported previously (42, 43), SET-Nup214 and
212 DEK-Nup214 are mainly localized in the nucleus as granular dots and influence
213 subcellular localization of XPO1. Because NXF1 was also co-immunoprecipitated
214 with SET-Nup214 and DEK-Nup214, we next examined subcellular localization of
215 both NTRs by indirect immunofluorescence (IF) assays. Endogenous XPO1 was
216 located in the nucleus and the nuclear envelope, whereas it was localized markedly as
217 granular dots upon expression of SET-Nup214 and DEK-Nup214 (Figure 1D).
218 XPO1 localization at the nuclear envelope in cells expressing Nup214 (1057-2090)
219 was reduced and mainly localized in the nucleus where Nup214 (1057-2090) existed.
220 Endogenous NXF1 was observed in the nucleus in control cells. On the other hand,
221 in cells expressing SET-Nup214, NXF1 was found in nuclear dots where
222 SET-Nup214 accumulated (Figure 1E), albeit the accumulation was less than XPO1.
223 In addition, in DEK-Nup214 expressing cells, we could not find clear accumulation of
224 NXF1 to the sites where DEK-Nup214 was accumulated. It was previously reported
225 that the FG repeat region of Nup214 plays crucial roles in binding with NTRs.
226 Therefore, we next examined the importance of the FG repeat region of the fusion
227 proteins for the localization changes of XPO1 and NFX1 using the deletion mutant of
228 SET-Nup214 termed SET-Nup214 (1637), which lacks the FG repeat region of
229 SET-Nup214. This mutant neither interacted with nor changed the localization of
230 both endogenous XPO1 and NXF1 (Figure 1C, lane 10, Figures 1D and 1E). These
231 results indicate that expression of SET-Nup214 and DEK-Nup214 affects the

localization pattern of both XPO1 and NXF1 by their physical interaction through the FG repeat region of Nup214.

NES proteins enhance dot formation of SET-Nup214 and DEK-Nup214

SET-Nup214 and DEK-Nup214 induced localization change of XPO1 and NXF1 through their physical interactions (Figure 1). NES proteins facilitate the interaction between XPO1 and Nup214 (38, 47, 48). To address the importance of NES proteins in the interaction between SET-Nup214 or DEK-Nup214 and NTRs, IP experiments were performed using cell lysates treated with or without leptomycin B (LMB), an inhibitor of binding between NES and XPO1(49). The amount of XPO1 co-immunoprecipitated with SET-Nup214 or DEK-Nup214 was decreased in LMB-treated cells (Figure 2A). In addition, granular dots generated by SET-Nup214 and DEK-Nup214 were decreased in size or disappeared after LMB addition (Figure 2B). These results suggest that the interaction of XPO1 and SET-Nup214 or DEK-Nup214 is under the control of its binding with NES proteins, and that the interaction between XPO1 and its cargos is indispensable for granular formation of SET-NUP214 and DEK-Nup214.

SET-Nup214 and DEK-Nup214 affect subcellular localization of endogenous proteins harboring NES

As XPO1 was accumulated in nuclear dots in cells expressing SET-Nup214 and DEK-Nup214 (Figure 1D), it was reasonable to hypothesize that intracellular availability of XPO1 may be decreased. We have previously found that EGFP fused to the NES of cAMP-dependent protein kinase inhibitor (PKI) was accumulated in the nucleus in cells expressing SET-Nup214 (43). However, it is not known whether

subcellular localization of endogenous NES proteins is actually affected by the expression of both SET-Nup214 and DEK-Nup214. Hence, we performed IF assays to observe endogenous XPO1 cargo proteins, IκBα and cyclin B1. IκBα (Figure 3A) and cyclin B1 (Figure 3C) were localized mainly in the cytoplasm in cells that did not express SET-Nup214 or DEK-Nup214. In contrast, they were uniformly accumulated in the nucleus upon expression of SET-Nup214 and DEK-Nup214. Because NF-κB transcription factor p65/RelA binds to IκBα in unstimulated cells, we examined the localization of p65 in cells expressing SET-Nup214 and DEK-Nup214. Interestingly, we found that the cytoplasmic localization of p65 was also disturbed by SET-Nup214 and DEK-Nup214. Quantitative analyses revealed that the ratio of fluorescent intensity of IκBα or p65 in the nucleus to that in the cytoplasm was increased significantly as intensity of SET-Nup214 and DEK-Nup214 increased (Figure 3A). When the C-terminal region of Nup214 (Nup214 (1057-2090)) was expressed, nuclear accumulation of IκBα and p65 was also observed (Figure 3B). It indicated that the C-terminal region of Nup214 can function as a dominant negative mutant of endogenous Nup214 as previously reported (39). From these observations, we conclude that SET-Nup214 and DEK-Nup214 change subcellular localization of endogenous proteins harboring NES by inhibiting the endogenous Nup214 function.

SET-Nup214 has a small effect on polyA mRNA localization

In addition to XPO1, the expression of SET-Nup214 affected the localization of NXF1, an NTR for mRNA (Figure 1E). We assessed subcellular localization pattern of mRNA by fluorescence *in situ* hybridization assays using oligo dT as a probe (Figure 3D). In control cells, oligo dT signal was observed both in the nucleus and the cytoplasm, and the cytoplasmic intensity was higher than the nuclear intensity. In

some of SET-Nup214 expressing cells, the signal intensity ratio of oligo dT in the nucleus to that in the cytoplasm is higher than that in control cells. Quantitative analyses showed that cells highly expressing SET-Nup214 were prone to mRNA accumulation in the nucleus. However, the accumulation of mRNAs was less clear than that of proteins harboring NES, suggesting that the effect of SET-Nup214 on the NXF1 function is lower than that on the XPO1 functions. In addition, we found that there was little difference of oligo dT staining pattern in control cells and cells expressing DEK-Nup214.

SET-Nup214 and DEK-Nup214 reduce the mobility of XPO1

Fluorescence Recovery After Photobleaching (FRAP) analyses have shown that XPO1 is highly mobile in the cell (50). As XPO1 is localized as granular dots in cells expressing SET-Nup214 and DEK-Nup214, it was possible that the XPO1 mobility was decreased. To test this, we performed FRAP assays for fluorescent protein-fused XPO1 (51), SET-Nup214, and DEK-Nup214. Expression of fluorescent proteins was confirmed by western blot analyses and immunofluorescence microscopy (Figures 4A and B). The area indicated by white square was bleached with 488 nm laser line, and intensity of the bleached area was monitored every 2 seconds. In control cells, the EGFP-XPO1 fluorescent intensity in the bleached area was restored rapidly after bleaching. On the other hand, EGFP-XPO1 was accumulated in the dots, and the recovery rate of fluorescence in the dots (indicated as yellow circle in Figure 4C) was significantly reduced by the co-expression of mKate2-SET-Nup214 and mKate2-DEK-Nup214. The intensity of mKate2-SET-Nup214 and mKate2-DEK-Nup214 after photobleaching was not efficiently recovered, and only a small fraction was recovered in 80 seconds (Figure

4C). These results indicate that SET-Nup214 and DEK-Nup214 in the dots are not exchangeable efficiently, but rather form stable complexes/aggregates to which XPO1 is attracted.

SET-Nup214 and DEK-Nup214 affect NF-κB transcription activity

We presumed that a cause of oncogenesis by the expression of SET-Nup214 and DEK-Nup214 is due at least in part to the deregulation of gene expression caused by aberrant localization of proteins and/or RNAs. Subcellular localization of p65 and IκBα was changed upon expression of SET-Nup214 and DEK-Nup214 (Figure 3A). It was reported Nup98-fusion proteins stimulate NFAT- and NF-κB-mediated transcription activities by impairing the XPO1 function (52). Thus, we examined the effect of these Nup214-fusion proteins on the NF-κB signaling pathway. The transcriptional activity of NF-κB was assessed first by reporter assays using firefly luciferase under the control of NF-κB (κB-FLuc). In the absence of TNF-α, the fusion proteins did not affect the luciferase activity (Figure 5A-C, left graphs), although the fusion proteins induced nuclear accumulation of p65 (Figure 3A). TNF-α treatment dramatically increased the reporter activity of κB-FLuc. This increase of the transcriptional activity was markedly inhibited by the expression of SET-Nup214 and DEK-Nup214 (Figure 5A-C, right graphs). As reported (53) (54) (55), LMB treatment showed an inhibitory effect on the luciferase activity of NF-κB-mediated transcription in the presence of TNF-α (Figure 5A-C, right graphs), while no significant effect was observed in the absence of TNF-α (Figure 5A-C, left graphs). The effects of SET-Nup214 and DEK-Nup214 expressions on the pTA-Renilla luciferase reporter under the control of the minimal promoter (TATA-RLuc) was less clear than those on the κB-luciferase activity, suggesting that

the effect of the expression of SET-Nup214 and DEK-Nup214 on the NF-κB-mediated transcription was specific. We next evaluated the effect of SET-Nup214 and DEK-Nup214 on the transcription of endogenous NF-κB target genes A20 and IκBα by RT-qPCR. Consistent with the reporter assays above, *set-nup214* and *dek-nup214* diminished the mRNA amounts of A20 and IκBα in a dose-dependent manner (Figure 5D). Collectively, these results demonstrate that SET-Nup214 and DEK-Nup214 impair the NF-κB transcription activity and this impairment occurs when the NF-κB signaling pathway is activated.

SET-Nup214 and DEK-Nup214 induce nuclear accumulation of the p65-IκBα complex in the absence of stimulus

In unstimulated cells, the majority of NF-κB transcription factors such as p65 and p50 interact with IκB. As p65 and p50 have NLS, and IκBα has NLS and NES, the NF-κB-IκBα complex shuttles between the nucleus and the cytoplasm in an XPO1-dependent manner and is mainly observed in the cytoplasm (53, 54, 56) (6, 55, 57, 58). In cells expressing SET-Nup214 and DEK-Nup214, the NF-κB transcription activity remained inactive (Figure 5C, left graph), despite p65 being located in the nucleus (Figure 3A). As IκBα is also localized in the nucleus, we hypothesized that the interaction between p65 and IκBα was maintained in the nucleus, and thus NF-κB was kept inactive. To test this, we performed *in situ* proximity ligation assays (PLA) and IP assays (Figures 6A and B). In control cells, p65 and IκBα were observed in the cytoplasm, and cytoplasmic PLA signals were detected, indicating the proximity of p65 and IκBα in the cytoplasm. When cells were transfected with *set-nup214* or *dek-nup214*, both p65 and IκBα were found in the nucleus (Figure 3A), and nuclear PLA signals were observed in these cells (Figure

6A). By IP assays, p65 was found to interact with IκBα, and this interaction was not affected by the absence or presence of SET-Nup214 and DEK-Nup214 (Figure 6B). These results suggest that SET-Nup214 and DEK-Nup214 induce nuclear accumulation of the p65-IκBα complex, but that the NF-κB signaling pathway was kept inactive, as the fusion proteins did not affect the interaction between p65 and IκBα. Binding of IκBα to p65 causes a release of p65 from DNA (59). Therefore, it was presumed that nuclear p65 bound by IκBα in the presence of SET-Nup214 and DEK-Nup214 could not bind to the target gene promoter. To confirm this notion, we performed chromatin immunoprecipitation assays. The level of p65 that bound to A20 and IκBα promoter regions was increased by TNF-α treatment. However, p65 binding to these promoters was not enhanced by SET-Nup214 and DEK-Nup214 (Figure 6C), although p65 was localized in the nucleus (Figure 3A). These results support our notion that p65 was kept inactive in cells expressing SET-Nup214 and DEK-Nup214.

p65-IκBα complex is kept in the presence of stimulus in cells expressing SET-Nup214 or DEK-Nup214

Reporter assays and RT-qPCR showed that SET-Nup214 and DEK-Nup214 down-regulate the NF-κB transcription activity in the presence of TNF-α (Figure 5C, right graph). IκBα is phosphorylated in the cytoplasm upon stimulation, followed by degradation by the ubiquitin proteasome system (60). NF-κB transcription factors are then freed from IκB, localized in the nucleus, and execute target gene transcription. We predicted that NF-κB-IκBα complex is maintained by the expression of SET-Nup214 and DEK-Nup214 even after TNF-α addition. To test this, the localization pattern of IκBα and p65 was monitored, and PLA and

co-immunoprecipitation assays were performed. After addition of TNF-α, IκBα in the cytoplasm of both control and SET-Nup214- and DEK-Nup214-expressing cells was markedly reduced (Figure 7A), indicating degradation of cytoplasmic IκBα. On the contrary, IκBα in the nucleus of SET-Nup214- and DEK-Nup214-expressing cells was visible after TNF-α treatment (Figure 7A). Restored expression level of IκBα by SET-Nup214 and DEK-Nup214 was also confirmed by western blotting analysis (Figure 7C, lanes 1-6). In cells expressing nuclear p65 and IκBα, PLA signals were detected both 0 and 30 minutes after TNF-α treatment, demonstrating that the interaction between p65 and IκBα was maintained in the nucleus after stimulation (Figure 7B). The p65-IκBα complex formation in stimulating cells expressing SET-Nup214 or DEK-Nup214 was confirmed by IP assay (Figure 7C, lanes 7-13). Finally, to examine whether the recruitment of p65 to its target genes was affected by SET-Nup214 or DEK-Nup214, ChIP assay was performed. It was demonstrated that p65 binding to the A20 and IκBα promoter regions was impaired in the presence of SET-Nup214 or DEK-Nup214 (Figure 7D). These results indicate that nuclear-localized IκBα induced by SET-Nup214 and DEK-Nup214 is escaped from its phosphorylation and degradation and keeps p65 inactive.

Subcellular localization of XPO1 and its cargos in *set-nup214* transgenic mice

Previously, we generated a transgenic mouse expressing *set-nup214* (22). Although this mouse did not develop leukemia, it shows severe anemia and a halt in hematopoietic differentiation, both of which are frequently associated with leukemia. In order to understand the biological relevance of the results obtained from *in vitro* cell culture studies, we assessed the localization pattern of XPO1 and its cargos using spleen sections from *set-nup214* transgenic mice. We observed that SET-Nup214

and XPO1 are co-localized in the nucleus as granular dots (Figure 8A). In addition, it was found that IκBα (Figure 8B) and p65 (Figure 8C) are also localized in the dots. These results demonstrate that the localization pattern of XPO1 is affected and its function could be impaired by SET-Nup214 *in vivo* as well.

411 **Discussion**

412

413 **Interaction of SET-Nup214 and DEK-Nup214 with XPO1 and NFX1**

414 In this study, we examined the function of SET-Nup214 and DEK-Nup214 in terms of
415 their effects on nuclear-cytoplasmic transport of proteins and RNAs. We found that
416 among several NTRs, SET-Nup214 and DEK-Nup214 interact preferentially with not
417 only XPO1 but also NXF1 (Figure 1B). These interactions were dependent on the
418 FG repeat region of SET-Nup214 and DEK-Nup214 (Figure 1C). It is shown that
419 each FG-Nup binds with different affinity to some of the NTRs, which contain
420 multiple binding sites for FG-repeats (61, 62). Hence, it is supposed that the
421 affinities of the FG repeat region of SET-Nup214 and DEK-Nup214 to NTRs are also
422 to be varied, and the affinity difference generates binding preference. Nup214
423 interacts with XPO1 rather than Xpo-t, NXF1, or XPO2/CAS (29, 63). Among
424 various NTRs, ectopic expression of truncated Nup214 containing FG repeat region
425 has an inhibitory effect on subset of NTRs functions including XPO1 (39). Our
426 results are consistent with previous ones, and imply that the SET and DEK portions of
427 the SET-Nup214 or DEK-Nup214 do not affect the structure and function of Nup214
428 portion for association with NTRs.

429

430 **Effects of SET-Nup214 and DEK-Nup214 on the functions of XPO1 and NXF1**

431 We have demonstrated that SET-Nup214 and DEK-Nup214 associate with both
432 XPO1 and NXF1. However, the effect of Nup214-fusion proteins on XPO1 function
433 was different from that on NXF1. We showed that SET-Nup214 and DEK-Nup214
434 induce lower mobility of XPO1 and cause accumulation of XPO1 cargos in the
435 nucleus (Figures 3A, C, and 4C). In contrast, mRNA, which is an NXF1 cargo, was

not accumulated in the nucleus of cells expressing SET-Nup214 and DEK-Nup214 (Figure 3D). XPO1 was mainly incorporated in the dots where SET-Nup214 and DEK-Nup214 are located, whereas nuclear-diffused NXF1 was observed in cells expressing SET-Nup214 and DEK-Nup214 (Figures 1D and E). This differential localization of XPO1 and NXF1 in cells expressing SET-Nup214 and DEK-Nup214 could explain the different effects of SET-Nup214 and DEK-Nup214 on the XPO1 and NXF1 functions. It is assumed that SET-Nup214-XPO1 and DEK-Nup214-XPO1 complexes could be more stable than SET-Nup214-NXF1 and DEK-Nup214-NXF1 complex.

SET-Nup214 and DEK-Nup214 form stable complexes with XPO1

A question is raised as to how SET-Nup214 and DEK-Nup214 can form a stable complex with XPO1 to induce accumulation of NES proteins in the nucleus. The interaction between Nup214 and XPO1 is stabilized when both RanGTP and NES proteins are incorporated (38, 47, 48). Consistent with this, we found that inhibition of the interaction between XPO1 and NES proteins by LMB leads to disappearance of dots formed in the presence of SET-Nup214 and DEK-Nup214 (Figure 2). From these results, we speculate that the nuclear dots are formed by the quaternary stable complex containing SET-Nup214 or DEK-Nup214, NES proteins, XPO1, and RanGTP. Furthermore, it is possible that other proteins play roles in the dot formation. Complex formation of RanGTP-XPO1-NES proteins is enhanced by Nup98 (64) and RanBP3 (65) (66) (67). Nup214 functions as a scaffold for the recruitment of several nucleoporins such as Nup88, Nup358, Nup62, and Nup98 (68) (38) (40, 69). These proteins may facilitate stable complex formation induced by SET-Nup214 and DEK-Nup214. In spleen cells, these dots are much larger than

those in cultured cells. It is likely that high expression of proteins constituting these dots in mouse spleen enlarges the SET-Nup214 nuclear dots.

Deregulation of transcription by SET-Nup214 and DEK-Nup214 and oncogenesis

We found that IκBα is localized in the nucleus regardless of the presence or absence of TNF-α (Figure 7A) in cells expressing SET-Nup214 and DEK-Nup214. It is presumed that nuclear-accumulation of IκBα is escaped from IKKβ-mediated phosphorylation after TNF-α addition, and thus the NF-κB transcription activity is repressed by the interaction with IκBα in the nucleus. In general, NF-κB induces transcription of various genes related to inflammation, cell proliferation, invasion, and so on. NF-κB inactivation is known to counteract oncogenesis or tumorigenesis and NF-κB is an efficient therapeutic target for cancer (70) (71). In contrast, NF-κB has also been reported to have anti-oncogenic activities, such as induction of cellular senescence. $p65^{-/-}$ MEFs bypass senescence (72), and p65-downregulated mouse lymphoma become chemoresistance by escape of senescence (73). SET-Nup214 and DEK-Nup214 impair the NF-κB pathway (Figure 5). On this line, it is speculated that SET-Nup214 and DEK-Nup214 may promote to bypass senescence via suppression of the NF-κB signaling pathway. In addition, several studies have documented the importance of the NF-κB pathway for hematopoiesis. Conditional knockout of IKKβ gene upregulates IL-1 production and stimulates proliferation of neutrophil progenitor, leading to neutrophilia and splenomegaly (74) (75). In addition, it was reported that conditional knockout of p65 or IKK β induces cell cycling of hematopoietic stem cells and increases their number (76) (77). These

observations suggest that inhibition of the NF-κB pathway is one potential cause of the SET-Nup214-induced differentiation block of hematopoietic progenitor cells observed in SET-Nup214 transgenic mice. Furthermore, it was previously demonstrated that the differentiation of U937 was inhibited by the expression of SET-Nup214 (23). Similarly, the differentiation of U937 was inhibited by the presence of IKKβ inhibitor (78) (79). These results also suggest that the inhibition of the NF-κB pathway by SET-Nup214 is, at least in part, a potential cause of U937 differentiation block induced by SET-Nup214.

In conclusion, SET-Nup214 and DEK-Nup214 interact with NTRs, and the interaction of either SET-Nup214 or DEK-Nup214 with XPO1 leads to a malfunction of transcription regulation by NF-κB. Until now, many proteins have been identified as XPO1 cargos (80) (81). In addition to IκBα and cyclin B1, these various cargos might accumulate in the nucleus of the case in which either SET-Nup214 or DEK-Nup214 is present. In fact, β-catenin was reported to accumulate in the nucleus of *set-nup214* transgenic mouse (21). Because appropriate nuclear-cytoplasmic transport is required to cellular integrity, these localization disturbances of various proteins may synergistically lead to oncogenesis by SET-Nup214 and DEK-Nup214. To know which NES proteins are responsible for SET-NUP214- and DEK-Nup214-mediated oncogenesis, comprehensive post-genome type analyses are required.

Acknowledgements

We thank Dr. Minoru Yoshida (RIKEN) for providing pHCF1 vector. We are grateful to Catherine Ann Moroski-Erkul for critical reading of this manuscript. This work was supported by JSPS KAKENHI Grant numbers 24790309 to S.S, 25291001 to K.N.)

References

1. **Walde S, Kehlenbach RH.** 2010. The Part and the Whole: functions of nucleoporins in nucleocytoplasmic transport. Trends in cell biology **20:**461-469.
2. **Strambio-De-Castillia C, Niepel M, Rout MP.** 2010. The nuclear pore complex: bridging nuclear transport and gene regulation. Nature reviews. Molecular cell biology **11:**490-501.
3. **Wente SR, Rout MP.** 2010. The nuclear pore complex and nuclear transport. Cold Spring Harbor perspectives in biology **2:**a000562.
4. **Kau TR, Way JC, Silver PA.** 2004. Nuclear transport and cancer: from mechanism to intervention. Nature reviews. Cancer **4:**106-117.
5. **O'Brate A, Giannakakou P.** 2003. The importance of p53 location: nuclear or cytoplasmic zip code? Drug resistance updates : reviews and commentaries in antimicrobial and anticancer chemotherapy **6:**313-322.
6. **Oeckinghaus A, Ghosh S.** 2009. The NF-kappaB family of transcription factors and its regulation. Cold Spring Harbor perspectives in biology **1:**a000034.
7. **Capelson M, Hetzer MW.** 2009. The role of nuclear pores in gene regulation, development and disease. EMBO reports **10:**697-705.
8. **Melo SA, Moutinho C, Ropero S, Calin GA, Rossi S, Spizzo R, Fernandez AF, Davalos V, Villanueva A, Montoya G, Yamamoto H, Schwartz S, Jr., Esteller M.** 2010. A genetic defect in exportin-5 traps precursor microRNAs in the nucleus of cancer cells. Cancer cell **18:**303-315.
9. **Puente XS, Pinyol M, Quesada V, Conde L, Ordonez GR, Villamor N, Escaramis G, Jares P, Bea S, Gonzalez-Diaz M, Bassaganyas L,**

Baumann T, Juan M, Lopez-Guerra M, Colomer D, Tubio JM, Lopez C, Navarro A, Tornador C, Aymerich M, Rozman M, Hernandez JM, Puente DA, Freije JM, Velasco G, Gutierrez-Fernandez A, Costa D, Carrio A, Guijarro S, Enjuanes A, Hernandez L, Yague J, Nicolas P, Romeo-Casabona CM, Himmelbauer H, Castillo E, Dohm JC, de Sanjose S, Piris MA, de Alava E, San Miguel J, Royo R, Gelpi JL, Torrents D, Orozco M, Pisano DG, Valencia A, Guigo R, Bayes M, Heath S, Gut M, Klatt P, Marshall J, Raine K, Stebbings LA, Futreal PA, Stratton MR, Campbell PJ, Gut I, Lopez-Guillermo A, Estivill X, Montserrat E, Lopez-Otin C, Campo E. 2011. Whole-genome sequencing identifies recurrent mutations in chronic lymphocytic leukaemia. Nature **475:**101-105.

10. **Jeromin S, Weissmann S, Haferlach C, Dicker F, Bayer K, Grossmann V, Alpermann T, Roller A, Kohlmann A, Haferlach T, Kern W, Schnittger S.** 2014. SF3B1 mutations correlated to cytogenetics and mutations in NOTCH1, FBXW7, MYD88, XPO1 and TP53 in 1160 untreated CLL patients. Leukemia **28:**108-117.

11. **Xu S, Powers MA.** 2009. Nuclear pore proteins and cancer. Seminars in cell & developmental biology **20:**620-630.

12. **Kohler A, Hurt E.** 2010. Gene regulation by nucleoporins and links to cancer. Molecular cell **38:**6-15.

13. **Funasaka T, Wong RW.** 2011. The role of nuclear pore complex in tumor microenvironment and metastasis. Cancer metastasis reviews **30:**239-251.

14. **Simon DN, Rout MP.** 2014. Cancer and the nuclear pore complex. Advances in experimental medicine and biology **773:**285-307.

15. **Zhou MH, Yang QM.** 2014. fusion genes in acute leukemia (Review). Oncology letters **8:**959-962.

16. **von Lindern M, Fornerod M, van Baal S, Jaegle M, de Wit T, Buijs A, Grosveld G.** 1992. The translocation (6;9), associated with a specific subtype of acute myeloid leukemia, results in the fusion of two genes, dek and can, and the expression of a chimeric, leukemia-specific dek-can mRNA. Molecular and cellular biology **12:**1687-1697.

17. **von Lindern M, van Baal S, Wiegant J, Raap A, Hagemeijer A, Grosveld G.** 1992. Can, a putative oncogene associated with myeloid leukemogenesis, may be activated by fusion of its 3' half to different genes: characterization of the set gene. Molecular and cellular biology **12:**3346-3355.

18. **Ben Abdelali R, Roggy A, Leguay T, Cieslak A, Renneville A, Touzart A, Banos A, Randriamalala E, Caillot D, Lioure B, Devidas A, Mossafa H, Preudhomme C, Ifrah N, Dombret H, Macintyre E, Asnafi V.** 2014. SET-NUP214 is a recurrent gammadelta lineage-specific fusion transcript associated with corticosteroid/chemotherapy resistance in adult T-ALL. Blood **123:**1860-1863.

19. **Sandahl JD, Coenen EA, Forestier E, Harbott J, Johansson B, Kerndrup G, Adachi S, Auvrignon A, Beverloo HB, Cayuela JM, Chilton L, Fornerod M, de Haas V, Harrison CJ, Inaba H, Kaspers GJ, Liang DC, Locatelli F, Masetti R, Perot C, Raimondi SC, Reinhardt K, Tomizawa D, von Neuhoff N, Zecca M, Zwaan CM, van den Heuvel-Eibrink MM,**

Hasle H. 2014. t(6;9)(p22;q34)/DEK-NUP214-rearranged pediatric myeloid leukemia: an international study of 62 patients. Haematologica **99:**865-872.

20. **Van Vlierberghe P, van Grotel M, Tchinda J, Lee C, Beverloo HB, van der Spek PJ, Stubbs A, Cools J, Nagata K, Fornerod M, Buijs-Gladdines J, Horstmann M, van Wering ER, Soulier J, Pieters R, Meijerink JP.** 2008. The recurrent SET-NUP214 fusion as a new HOXA activation mechanism in pediatric T-cell acute lymphoblastic leukemia. Blood **111:**4668-4680.

21. **Ozbek U, Kandilci A, van Baal S, Bonten J, Boyd K, Franken P, Fodde R, Grosveld GC.** 2007. SET-CAN, the product of the t(9;9) in acute undifferentiated leukemia, causes expansion of early hematopoietic progenitors and hyperproliferation of stomach mucosa in transgenic mice. The American journal of pathology **171:**654-666.

22. **Saito S, Nouno K, Shimizu R, Yamamoto M, Nagata K.** 2008. Impairment of erythroid and megakaryocytic differentiation by a leukemia-associated and t(9;9)-derived fusion gene product, SET/TAF-Ibeta-CAN/Nup214. Journal of cellular physiology **214:**322-333.

23. **Kandilci A, Mientjes E, Grosveld G.** 2004. Effects of SET and SET-CAN on the differentiation of the human promonocytic cell line U937. Leukemia **18:**337-340.

24. **Ageberg M, Drott K, Olofsson T, Gullberg U, Lindmark A.** 2008. Identification of a novel and myeloid specific role of the leukemia-associated fusion protein DEK-NUP214 leading to increased protein synthesis. Genes, chromosomes & cancer **47:**276-287.

25. **Sanden C, Ageberg M, Petersson J, Lennartsson A, Gullberg U.** 2013. Forced expression of the DEK-NUP214 fusion protein promotes proliferation dependent on upregulation of mTOR. BMC cancer **13:**440.

26. **Oancea C, Ruster B, Henschler R, Puccetti E, Ruthardt M.** 2010. The t(6;9) associated DEK/CAN fusion protein targets a population of long-term repopulating hematopoietic stem cells for leukemogenic transformation. Leukemia **24:**1910-1919.

27. **Moroianu J, Hijikata M, Blobel G, Radu A.** 1995. Mammalian karyopherin alpha 1 beta and alpha 2 beta heterodimers: alpha 1 or alpha 2 subunit binds nuclear localization signal and beta subunit interacts with peptide repeat-containing nucleoporins. Proceedings of the National Academy of Sciences of the United States of America **92:**6532-6536.

28. **Boer J, Bonten-Surtel J, Grosveld G.** 1998. Overexpression of the nucleoporin CAN/NUP214 induces growth arrest, nucleocytoplasmic transport defects, and apoptosis. Molecular and cellular biology **18:**1236-1247.

29. **Kuersten S, Arts GJ, Walther TC, Englmeier L, Mattaj IW.** 2002. Steady-state nuclear localization of exportin-t involves RanGTP binding and two distinct nuclear pore complex interaction domains. Molecular and cellular biology **22:**5708-5720.

30. **Fornerod M, van Deursen J, van Baal S, Reynolds A, Davis D, Murti KG, Fransen J, Grosveld G.** 1997. The human homologue of yeast CRM1 is in a dynamic subcomplex with CAN/Nup214 and a novel nuclear pore component Nup88. The EMBO journal **16:**807-816.

31. **Katahira J, Strasser K, Podtelejnikov A, Mann M, Jung JU, Hurt E.** 1999. The Mex67p-mediated nuclear mRNA export pathway is conserved from yeast to human. The EMBO journal **18:**2593-2609.

32. **Bachi A, Braun IC, Rodrigues JP, Pante N, Ribbeck K, von Kobbe C, Kutay U, Wilm M, Gorlich D, Carmo-Fonseca M, Izaurralde E.** 2000. The C-terminal domain of TAP interacts with the nuclear pore complex and promotes export of specific CTE-bearing RNA substrates. RNA (New York, N.Y.) **6:**136-158.

33. **Levesque L, Guzik B, Guan T, Coyle J, Black BE, Rekosh D, Hammarskjold ML, Paschal BM.** 2001. RNA export mediated by tap involves NXT1-dependent interactions with the nuclear pore complex. The Journal of biological chemistry **276:**44953-44962.

34. **Wiegand HL, Coburn GA, Zeng Y, Kang Y, Bogerd HP, Cullen BR.** 2002. Formation of Tap/NXT1 heterodimers activates Tap-dependent nuclear mRNA export by enhancing recruitment to nuclear pore complexes. Molecular and cellular biology **22:**245-256.

35. **Herold A, Suyama M, Rodrigues JP, Braun IC, Kutay U, Carmo-Fonseca M, Bork P, Izaurralde E.** 2000. TAP (NXF1) belongs to a multigene family of putative RNA export factors with a conserved modular architecture. Molecular and cellular biology **20:**8996-9008.

36. **van Deursen J, Boer J, Kasper L, Grosveld G.** 1996. G2 arrest and impaired nucleocytoplasmic transport in mouse embryos lacking the proto-oncogene CAN/Nup214. The EMBO journal **15:**5574-5583.

37. **Bernad R, Engelsma D, Sanderson H, Pickersgill H, Fornerod M.** 2006. Nup214-Nup88 nucleoporin subcomplex is required for CRM1-mediated

60 S preribosomal nuclear export. The Journal of biological chemistry **281:**19378-19386.

38. **Hutten S, Kehlenbach RH.** 2006. Nup214 is required for CRM1-dependent nuclear protein export in vivo. Molecular and cellular biology **26:**6772-6785.

39. **Roloff S, Spillner C, Kehlenbach RH.** 2013. Several phenylalanine-glycine motives in the nucleoporin Nup214 are essential for binding of the nuclear export receptor CRM1. The Journal of biological chemistry **288:**3952-3963.

40. **Xylourgidis N, Roth P, Sabri N, Tsarouhas V, Samakovlis C.** 2006. The nucleoporin Nup214 sequesters CRM1 at the nuclear rim and modulates NFkappaB activation in Drosophila. Journal of cell science **119:**4409-4419.

41. **Takeda A, Yaseen NR.** 2014. Nucleoporins and nucleocytoplasmic transport in hematologic malignancies. Seminars in cancer biology **27:**3-10.

42. **Fornerod M, Boer J, van Baal S, Morreau H, Grosveld G.** 1996. Interaction of cellular proteins with the leukemia specific fusion proteins DEK-CAN and SET-CAN and their normal counterpart, the nucleoporin CAN. Oncogene **13:**1801-1808.

43. **Saito S, Miyaji-Yamaguchi M, Nagata K.** 2004. Aberrant intracellular localization of SET-CAN fusion protein, associated with a leukemia, disorganizes nuclear export. International journal of cancer. Journal international du cancer **111:**501-507.

44. **Nagata K, Saito S, Okuwaki M, Kawase H, Furuya A, Kusano A, Hanai N, Okuda A, Kikuchi A.** 1998. Cellular localization and expression of template-activating factor I in different cell types. Experimental cell research **240:**274-281.

45. **Numajiri Haruki A, Naito T, Nishie T, Saito S, Nagata K.** 2011. Interferon-inducible antiviral protein MxA enhances cell death triggered by endoplasmic reticulum stress. Journal of interferon & cytokine research : the official journal of the International Society for Interferon and Cytokine Research **31:**847-856.

46. **Herold A, Klymenko T, Izaurralde E.** 2001. NXF1/p15 heterodimers are essential for mRNA nuclear export in Drosophila. RNA (New York, N.Y.) **7:**1768-1780.

47. **Askjaer P, Bachi A, Wilm M, Bischoff FR, Weeks DL, Ogniewski V, Ohno M, Niehrs C, Kjems J, Mattaj IW, Fornerod M.** 1999. RanGTP-regulated interactions of CRM1 with nucleoporins and a shuttling DEAD-box helicase. Molecular and cellular biology **19:**6276-6285.

48. **Kehlenbach RH, Dickmanns A, Kehlenbach A, Guan T, Gerace L.** 1999. A role for RanBP1 in the release of CRM1 from the nuclear pore complex in a terminal step of nuclear export. The Journal of cell biology **145:**645-657.

49. **Kudo N, Wolff B, Sekimoto T, Schreiner EP, Yoneda Y, Yanagida M, Horinouchi S, Yoshida M.** 1998. Leptomycin B inhibition of signal-mediated nuclear export by direct binding to CRM1. Experimental cell research **242:**540-547.

50. **Daelemans D, Costes SV, Lockett S, Pavlakis GN.** 2005. Kinetic and molecular analysis of nuclear export factor CRM1 association with its cargo in vivo. Molecular and cellular biology **25:**728-739.

51. **Kudo N, Khochbin S, Nishi K, Kitano K, Yanagida M, Yoshida M, Horinouchi S.** 1997. Molecular cloning and cell cycle-dependent expression of mammalian CRM1, a protein involved in nuclear export of proteins. The Journal of biological chemistry **272:**29742-29751.

52. **Takeda A, Sarma NJ, Abdul-Nabi AM, Yaseen NR.** 2010. Inhibition of CRM1-mediated nuclear export of transcription factors by leukemogenic NUP98 fusion proteins. The Journal of biological chemistry **285:**16248-16257.

53. **Johnson C, Van Antwerp D, Hope TJ.** 1999. An N-terminal nuclear export signal is required for the nucleocytoplasmic shuttling of IkappaBalpha. The EMBO journal **18:**6682-6693.

54. **Rodriguez MS, Thompson J, Hay RT, Dargemont C.** 1999. Nuclear retention of IkappaBalpha protects it from signal-induced degradation and inhibits nuclear factor kappaB transcriptional activation. The Journal of biological chemistry **274:**9108-9115.

55. **Huang TT, Kudo N, Yoshida M, Miyamoto S.** 2000. A nuclear export signal in the N-terminal regulatory domain of IkappaBalpha controls cytoplasmic localization of inactive NF-kappaB/IkappaBalpha complexes. Proceedings of the National Academy of Sciences of the United States of America **97:**1014-1019.

56. **Tam WF, Lee LH, Davis L, Sen R.** 2000. Cytoplasmic sequestration of rel proteins by IkappaBalpha requires CRM1-dependent nuclear export. Molecular and cellular biology **20:**2269-2284.

57. **Malek S, Chen Y, Huxford T, Ghosh G.** 2001. IkappaBbeta, but not IkappaBalpha, functions as a classical cytoplasmic inhibitor of NF-kappaB dimers by masking both NF-kappaB nuclear localization sequences in resting cells. The Journal of biological chemistry **276:**45225-45235.

58. **Hayden MS, Ghosh S.** 2004. Signaling to NF-kappaB. Genes & development **18:**2195-2224.

59. **Baeuerle PA, Baltimore D.** 1988. I kappa B: a specific inhibitor of the NF-kappa B transcription factor. Science (New York, N.Y.) **242:**540-546.

60. **Kanarek N, Ben-Neriah Y.** 2012. Regulation of NF-kappaB by ubiquitination and degradation of the IkappaBs. Immunological reviews **246:**77-94.

61. **Allen NP, Huang L, Burlingame A, Rexach M.** 2001. Proteomic analysis of nucleoporin interacting proteins. The Journal of biological chemistry **276:**29268-29274.

62. **Terry LJ, Wente SR.** 2009. Flexible gates: dynamic topologies and functions for FG nucleoporins in nucleocytoplasmic transport. Eukaryotic cell **8:**1814-1827.

63. **Kang Y, Bogerd HP, Cullen BR.** 2000. Analysis of cellular factors that mediate nuclear export of RNAs bearing the Mason-Pfizer monkey virus constitutive transport element. Journal of virology **74:**5863-5871.

64. **Oka M, Asally M, Yasuda Y, Ogawa Y, Tachibana T, Yoneda Y.** 2010. The mobile FG nucleoporin Nup98 is a cofactor for Crm1-dependent protein export. Molecular biology of the cell **21:**1885-1896.

65. **Englmeier L, Fornerod M, Bischoff FR, Petosa C, Mattaj IW, Kutay U.** 2001. RanBP3 influences interactions between CRM1 and its nuclear protein export substrates. EMBO reports **2:**926-932.

66. **Lindsay ME, Holaska JM, Welch K, Paschal BM, Macara IG.** 2001. Ran-binding protein 3 is a cofactor for Crm1-mediated nuclear protein export. The Journal of cell biology **153:**1391-1402.

67. **Koyama M, Shirai N, Matsuura Y.** 2014. Structural insights into how Yrb2p accelerates the assembly of the Xpo1p nuclear export complex. Cell reports **9:**983-995.

68. **Bernad R, van der Velde H, Fornerod M, Pickersgill H.** 2004. Nup358/RanBP2 attaches to the nuclear pore complex via association with Nup88 and Nup214/CAN and plays a supporting role in CRM1-mediated nuclear protein export. Molecular and cellular biology **24:**2373-2384.

69. **Schwartz M, Travesa A, Martell SW, Forbes DJ.** 2015. Analysis of the initiation of nuclear pore assembly by ectopically targeting nucleoporins to chromatin. Nucleus (Austin, Tex.) **6:**40-54.

70. **Prasad S, Ravindran J, Aggarwal BB.** 2010. NF-kappaB and cancer: how intimate is this relationship. Molecular and cellular biochemistry **336:**25-37.

71. **Perkins ND.** 2007. Integrating cell-signalling pathways with NF-kappaB and IKK function. Nature reviews. Molecular cell biology **8:**49-62.

781 72. **Wang J, Jacob NK, Ladner KJ, Beg A, Perko JD, Tanner SM,**
782 **Liyanarachchi S, Fishel R, Guttridge DC.** 2009. RelA/p65 functions to
783 maintain cellular senescence by regulating genomic stability and DNA
784 repair. EMBO reports **10:**1272-1278.
785 73. **Chien Y, Scuoppo C, Wang X, Fang X, Balgley B, Bolden JE, Premsrirut**
786 **P, Luo W, Chicas A, Lee CS, Kogan SC, Lowe SW.** 2011. Control of the
787 senescence-associated secretory phenotype by NF-kappaB promotes
788 senescence and enhances chemosensitivity. Genes & development
789 **25:**2125-2136.
790 74. **Hsu LC, Enzler T, Seita J, Timmer AM, Lee CY, Lai TY, Yu GY, Lai LC,**
791 **Temkin V, Sinzig U, Aung T, Nizet V, Weissman IL, Karin M.** 2011.
792 IL-1beta-driven neutrophilia preserves antibacterial defense in the
793 absence of the kinase IKKbeta. Nature immunology **12:**144-150.
794 75. **Mankan AK, Canli O, Schwitalla S, Ziegler P, Tschopp J, Korn T, Greten**
795 **FR.** 2011. TNF-alpha-dependent loss of IKKbeta-deficient myeloid
796 progenitors triggers a cytokine loop culminating in granulocytosis.
797 Proceedings of the National Academy of Sciences of the United States of
798 America **108:**6567-6572.
799 76. **Stein SJ, Baldwin AS.** 2013. Deletion of the NF-kappaB subunit p65/RelA
800 in the hematopoietic compartment leads to defects in hematopoietic stem
801 cell function. Blood **121:**5015-5024.
802 77. **Zhang J, Li L, Baldwin AS, Jr., Friedman AD, Paz-Priel I.** 2015. Loss of
803 IKKbeta but Not NF-kappaB p65 Skews Differentiation towards Myeloid
804 over Erythroid Commitment and Increases Myeloid Progenitor

Self-Renewal and Functional Long-Term Hematopoietic Stem Cells. PloS one **10:**e0130441.

78. **Dai Y, Rahmani M, Grant S.** 2003. An intact NF-kappaB pathway is required for histone deacetylase inhibitor-induced G1 arrest and maturation in U937 human myeloid leukemia cells. Cell cycle (Georgetown, Tex.) **2:**467-472.

79. **Song MG, Ryoo IG, Choi HY, Choi BH, Kim ST, Heo TH, Lee JY, Park PH, Kwak MK.** 2015. NRF2 Signaling Negatively Regulates Phorbol-12-Myristate-13-Acetate (PMA)-Induced Differentiation of Human Monocytic U937 Cells into Pro-Inflammatory Macrophages. PloS one **10:**e0134235.

80. **Fu SC, Huang HC, Horton P, Juan HF.** 2013. ValidNESs: a database of validated leucine-rich nuclear export signals. Nucleic acids research **41:**D338-343.

81. **Thakar K, Karaca S, Port SA, Urlaub H, Kehlenbach RH.** 2013. Identification of CRM1-dependent Nuclear Export Cargos Using Quantitative Mass Spectrometry. Molecular & cellular proteomics : MCP **12:**664-678.

82. **Okuwaki M, Sumi A, Hisaoka M, Saotome-Nakamura A, Akashi S, Nishimura Y, Nagata K.** 2012. Function of homo- and hetero-oligomers of human nucleoplasmin/nucleophosmin family proteins NPM1, NPM2 and NPM3 during sperm chromatin remodeling. Nucleic acids research **40:**4861-4878.

Figure legends

Figure 1 Interaction between SET-Nup214 and DEK-Nup214 proteins and NTRs. (A) Schematic representation of SET-Nup214, DEK-Nup214, Nup214 (1057-2090), and SET-Nup214 (1637) used in our study and full length Nup214. Box with vertical bars, SET portion; box with black dots, DEK portion; gray box, FG repeat region. (B) HEK293T cells cultured in 6-well plates were transfected with 1 μg of pCHA-nuclear transport receptors (NTRs) or pCAGGS and 1 μg of pCAGGS-SET-Nup214-3Flag, DEK-Nup214-3Flag, or 3Flag-Nup214 (1057-2090). At two days after transfection, cells were collected and subjected to IP assays with 300 ng of anti-HA (3F10) High Affinity antibody (Roche Diagnostics GmbH), and immunocomplexes were recovered by nProtein A Sepharose Fast Flow (GE Healthcare UK Ltd.). After IP assays, proteins in input lysates and immunoprecipitated samples were separated by 6% SDS-PAGE, and western blot analyses were performed using anti-Flag M2 (2 μg/ml) (Sigma-Aldrich Co. LLC), and anti-HA (3F10) (1:1000) antibodies. Prestained molecular weight markers (kDa) (Nacalai tesque, Inc., Japan) are indicated in the left. (C) HEK293T cells cultured in 10-cm dishes were transfected with 5 μg of pCAGGS, SET-Nup214-3Flag, DEK-Nup214-3Flag, 3Flag-Nup214 (1057-2090), and 3Flag-SET-Nup214 (1637). At two days after transfection, cells were collected, and cell lysates were subjected to immunoprecipitation with anti-Flag M2 Agarose Affinity Gel (Sigma-Aldrich Co. LLC.). Proteins in input lysates and immunoprecipitated samples were separated by 6.5%SDS-PAGE, and western blot analyses were performed using anti-Flag, anti-XPO1 (H-300) (1:1000) (Santa Cruz Biotechnology, Inc.), anti-NXF1 (53H8, Santa Cruz Biotechnology, Inc.) (1:500), and anti-β-actin (AC-15, Sigma-Aldrich Co. LLC) (1:5000) antibodies. Prestained molecular weight markers (kDa) are indicated

855 in the left. (D, E) HeLa cells cultured in 35-mm dishes were transfected with pCHA,
856 HA-SET-Nup214, HA-DEK-Nup214, HA-Nup214 (1057-2090), and
857 HA-SET-Nup214 (1637). At two days after transfection, cells were subjected to IF
858 assays. For primary antibody, anti-HA (3F10) (1:100) (D), anti-XPO1 (1:20) (D),
859 anti-HA rabbit (1:500) (E), and anti-NXF1 (1:20) (E) antibodies were used. Right
860 graphs represent relative intensities of HA-tagged protein and XPO1 (D) or NXF1 (E)
861 along a line. Bar: 10 μm.
862
863 **Figure 2 Dependency of NES proteins on complex and dot formation of either**
864 **SET-Nup214 or DEK-Nup214 with XPO1.** (A) HeLa cells cultured in 35-mm
865 dishes were transiently transfected with 1 μg of either pCAGGS-SET-Nup214-3Flag
866 (SET-N214), DEK-Nup214-3Flag (DEK-N214), or pCAGGS. At two days after
867 transfection, cells were incubated in 5 ng/ml LMB (L-6100, LC Laboratories) for 0
868 and 6 h. After incubation, cells were collected, and subjected to IP assays using
869 FLAG M2 beads (lanes 6 to 13). Proteins in input lysate and immunoprecipitated
870 samples were separated by 6.5% SDS-PAGE, and western blot analyses were
871 performed using anti-FLAG, anti-XPO1 antibodies as primary antibodies.
872 Prestained molecular weight markers (kDa) are indicated in the left. (B) Protocol
873 was the same as one for Figure 2A. After cells were collected, IF analyses were
874 performed. For primary antibody, anti-Flag M2 (1:1000) and anti-XPO1 antibodies
875 were used. Right graphs represent relative intensities of Flag-tagged protein and
876 XPO1 along a line. Bar: 20 μm.
877
878 **Figure 3 Localization of endogenous proteins harboring NES and mRNA.** (A)
879 (Pictures) HeLa cells were transiently transfected with pCHA-SET-Nup214 or

HA-DEK-Nup214, and subjected to IF assays using anti-HA (3F10), anti-IκBα (C-21, Santa Cruz Biotechnology, Inc.) (1:100) or anti-p65 (PC137, Calbiochem) (1:100) antibodies. (Graphs) Fluorescence intensity was quantitatively determined using ImageJ software. Nuclear and cytoplasmic areas were selected manually. X axis=mean (intensity of HA-tagged protein in the nucleus)-mean(background), and Y axis=N/C=(mean(intensity of IκBα or p65 in the nucleus)-mean (background))/(mean (intensity of IκBα or p65 in the cytoplasm)-mean(background)). (B) 293T cells were transfected with pCHA, HA-SET-Nup214, HA-DEK-Nup214, HA-Nup214 (1057-2090), HA-SET-Nup214 (1637). Two days later, cells were subjected to immunofluorescence assay using anti-HA (3F10) and anti-IκBα (L35A5, CST, Inc.) (1:20) antibodies. Fluorescence intensities of nuclear IκBα and HA-tagged protein in each sample were quantitatively determined using ImageJ software and plotted. Bar: 20 μm. (C) HeLa cells were transiently transfected with pCHA-SET-Nup214 or DEK-Nup214, and subjected to IF assays using anti-HA (3F10), and anti-cyclinB1 (4138, CST Inc.) (1:20) antibodies. Fluorescence intensity of nuclear cyclin B1 in each cell was quantitatively determined using ImageJ software and plotted. Bar: 20 μm. $*P < 0.005$, $**P < 0.0005$. (D) HeLa cells were transiently transfected with pCAGGS, SET-Nup214-3Flag, or DEK-Nup214-3Flag, and subjected to IF assays using anti-Flag M2, and *in situ* hybridization assay with 10 ng/μl biotinylated oligo dT_{45} or oligo dA_{45} as probes. In the dot plots, fluorescence intensity was quantified using ImageJ software as described in Figure 3A. Bar: 10 μm.

Figure 4 Decreased mobility of XPO1. (A) HEK293T cells cultured in 35-mm dishes were transiently transfected with 1 μg pHCF1 (XPO1-EGFP expression vector), pmKate2C-SET-Nup214, and pmKate2C-DEK-Nup214. Samples were separated by

905 5% SDS-PAGE and subjected to western blot analyses using anti-Nup214 (1:1000),
906 anti-XPO1, and anti-C23 (D6, Santa Cruz Biotechnology, Inc.) (1:1000) antibodies.
907 Prestained molecular weight markers (kDa) are indicated in the left. (B, C) HeLa
908 cells were transfected with 1 μg pHCF1, and 1 μg pmKate2C,
909 pmKate2C-SET-Nup214, or pmKate2C-DEK-Nup214 and subjected to FRAP assays
910 (C) as previously described (82). Typical localization patterns of EGFP-XPO1,
911 mKate2, mKate2-SET-Nup214, and mKate2-DEK-Nup214 are shown in (B). Bar:
912 10 μm.
913
914 **Figure 5 Effects of SET-Nup214 and DEK-Nup214 on NF-κB transcription**
915 **activity.** (A-C) HEK293T cells ($3x10^4$) cultured in 24-well plates were transfected
916 with pNF-κB40-firefly luciferase (10 ng), and pCAGGS-SET-Nup214 (SET-N214) or
917 DEK-Nup214 (DEK-N214) (10, 100 ng). pTA-Renilla luciferase (100 ng) was
918 co-transfected for normalization of transfection efficiency. At two days after
919 transfection, cells were incubated with 1 ng/ml (lane 6 in left graphs and lane 7 in
920 right graphs) or 5 ng/ml LMB (lane 7 in left graphs and lane 8 in right graphs) for 30
921 min. Then, recombinant human TNF-α (300-01A, PeproTech) was added, at the
922 final concentration as 20 ng/ml (lanes 2-8 in right graphs), incubated for 3-4 h, and
923 cell lysates were subjected to luciferase assays using Dual-Luciferase Reporter Assay
924 System (Promega) according to manufacturer's instructions. Luminescence was
925 measured by CentroXS^3 LB960 (Berthold Japan K.K.). Relative luciferase activity
926 of the firefly luciferase activity (A), Renilla luciferase activity (B), and normalized
927 luciferase activity (C) were expressed as fold activation relative to lane 1. Data are
928 presented as the mean ± SD of three independent experiments. *P* value was
929 calculated with lane 1 (left graph) or lane 2 (right graph). $*P < 0.05$, $**P < 0.005$,

930 ***$P < 0.001$. Western blot analyses were performed using lysate prepared for
931 luciferase assays in the presence of TNF-α. Anti-Nup214 and anti-C23 antibodies
932 were used as primary antibodies. Prestained molecular weight markers (kDa) are
933 indicated in the left. (D) HEK293T cells ($3x10^5$) cultured in 6-well plates were
934 transfected with pCAGGS-SET-Nup214 (SET-N214) or DEK-Nup214 (DEK-N214)
935 (100, 1000 ng). At two days after transfection, cells were incubated with 5 ng/ml
936 LMB (lane 7) for 30 min, and TNF-α was added at the final concentration as 20 ng/ml
937 (lanes 2-7). After TNF-α incubation for 3-4 h, cells were collected, and isolated
938 RNAs were subjected to RT-qPCR to measure A20 and IκBα mRNAs. These
939 mRNA expression levels were normalized to the level of β-actin mRNA and shown as
940 fold inhibition relative to lane 2. Data are presented as the mean ± SD of three
941 independent experiments. *P* value was calculated with lane 2. *$P < 0.05$,
942 **$P < 0.005$, ***$P < 0.001$.
943
944 **Figure 6 Interaction of p65 with IκBα or chromatin in the nucleus.** (A) HeLa
945 cells cultured in 6-cm dishes were transfected with 2 μg pCHA, HA-SET-Nup214
946 (SET-N214), or HA-DEK-Nup214 (DEK-N214). At two days after transfection, cells
947 were collected, and subjected to IF assays and PLA. Anti-p65 (ab7970, Abcam)
948 (1:100) and anti-IκBα (L35A5, CST, Inc.) (1:30) antibodies were used for primary
949 antibodies. Merged is a composite picture stained with Alexa 488, Detection
950 Reagents Red (for PLA), and Alexa 633. Bar: 10 μm. (B) HEK293T cells were
951 transfected with pCAGGS, pCAGGS-SET-Nup214 (SN214),
952 pCAGGS-DEK-Nup214 (DN214) (0.2, 2 μg), and incubated for 2 days. Cells were
953 collected, and IP assays were conducted using anti-p65 (ab7970) and rabbit IgG
954 polyclonal antibodies (PP64B) (Merck KGaA, Germany). Proteins in input lysates

955 and immunoprecipitated samples were separated by 10% or 5% SDS-PAGE, and
956 western blot analyses were performed using anti-p65, anti-IκBα, anti-Nup214, and
957 anti-C23 antibodies. Molecular weights (kDa) of prestained markers are indicated in
958 the right. (C) HEK293T cells were transfected with 5 μg pCAGGS,
959 pCAGGS-SET-Nup214 (SET-N214), or pCAGGS-DEK-Nup214 (DEK-N214). At
960 two days after transfection, cells were treated with or without TNF-α (20 ng/ml) for
961 30 min, and then subjected to ChIP assays using 2 μg anti-IgG or anti-p65 (ab7970)
962 antibodies to measure p65 binding to A20 and IκBα promoter regions. The
963 immunoprecipitated DNA levels were normalized to the input DNA level and shown
964 as fold activation relative to immunoprecipitated DNA from pCAGGS-transfected
965 lysates by anti-p65 antibody in the absence of TNFα. Data are presented as the
966 mean ± SD of three independent experiments. *$P < 0.05$.
967
968 **Figure 7 Interaction of p65 with IκBα or chromatin in the presence of stimuli.**
969 (A) HeLa cells were transfected with 1 μg of pCHA, HA-SET-Nup214, or
970 HA-DEK-Nup214. At two days after transfection, cells were treated with TNF-α
971 (10 ng/ml) 30 min, and IF assays were performed using anti-HA rabbit and anti-IκBα
972 (L35A5) antibodies. Fluorescence intensity of nuclear IκBα in control cells,
973 SET-Nup214 expressing cells, and DEK-Nup214 expressing cells was quantitatively
974 determined using ImageJ software. Bar: 20 μm. ***$P < 0.001$. (B) The protocol
975 was the same as one for Figure 7A. After incubation with anti-p65 (ab7970) and
976 anti-IκBα (L35A5), PLA were performed. Merged is a composite picture stained
977 with Alexa 488, Detection Reagents Red (for PLA), and Alexa 633. Sum of
978 fluorescence intensity of PLA dots in each cell was quantitated using ImageJ software.
979 Bar: 10 μm. **$P < 0.005$, ***$P < 0.001$. (C) HEK293T cells were transfected with

1 μg pCAGGS, pCAGGS-SET-Nup214 (SN214), pCAGGS-DEK-Nup214 (DN214) (0.2, 2 μg). At two days after transfection, cells were treated with TNF-α (20 ng/ml) 30 min, collected, and IP assays were conducted using anti-p65 (ab7970) and rabbit IgG polyclonal antibodies. Proteins in input lysates and immunoprecipitated samples were separated by 12.5% or 5% SDS-PAGE, and western blot analyses were performed using anti-p65, anti-IκBα, anti-Nup214, and anti-C23 antibodies. Molecular weights (kDa) of prestained markers are indicated in the right. (D) HEK293T cells were transfected with 2 μg pCAGGS, pCAGGS-SET-Nup214 (SET-N214), or pCAGGS-DEK-Nup214 (DEK-N214). At two days after transfection, cells were treated with or without TNF-α (20 ng/ml) for 60 min, and then subjected to ChIP assays same as Figure 6C. Left graph represents the typical example and the right graph represents fold inhibition relative to immunoprecipitated DNA from pCAGGS-transfected lysates by anti-p65 antibody in the presence of TNF–α. Right graphs are presented as the mean ± SD of three independent experiments. $*P < 0.05$, $**P < 0.01$.

Figure 8 Subcellular localization of XPO1, IκBα, and p65 in spleen of *set-nup214* transgenic mice. Spleen sections of wild-type BDF1 and *set-nup214* transgenic mice (lines G79 and G593) were subjected to IF assays. Anti-SET/TAF-Iβ (KM1721) (1:20) (A), anti-XPO1 (1:100) (A), anti-Nup214 (1:100) (B, C), anti-IκBα (L35A5) (1:20) (B), and anti-p65 (F6) (1:20) (C), antibodies were used as primary antibodies. Merged is a composite picture stained with Alexa 488, Alexa 568, and TOPRO-3. Bar: 5 μm (A, C), 10 μm (B).

Figure 1

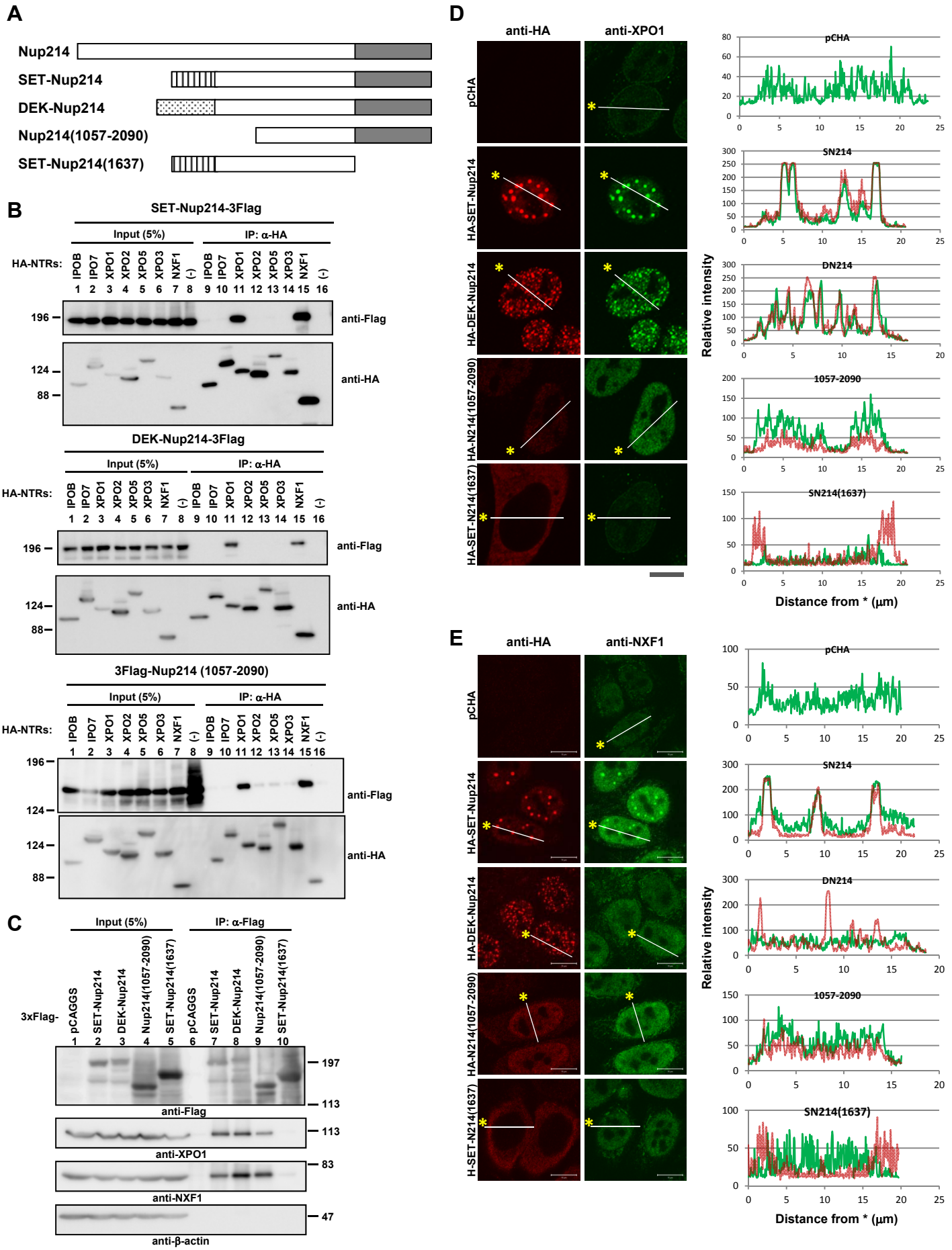
A
Nup214
SET-Nup214
DEK-Nup214
Nup214(1057-2090)
SET-Nup214(1637)
B
SET-Nup214-3Flag
Input (5%)
IP: α-HA
HA-NTRs:
IPOB IPO7 XPO1 XPO2 XPO5 XPO3 NXF1 (-)
1 2 3 4 5 6 7 8 9 10 11 12 13 14 15 16
196
anti-Flag
124
88
anti-HA
DEK-Nup214-3Flag
3Flag-Nup214 (1057-2090)
C
Input (5%)
IP: α-Flag
3xFlag-
pCAGGS SET-Nup214 DEK-Nup214 Nup214(1057-2090) SET-Nup214(1637)
1 2 3 4 5 6 7 8 9 10
anti-Flag
anti-XPO1
anti-NXF1
anti-β-actin
197
113
83
47
D
anti-HA
anti-XPO1
pCHA
HA-SET-Nup214
HA-DEK-Nup214
HA-N214(1057-2090)
HA-SET-N214(1637)
Relative intensity
SN214
DN214
1057-2090
SN214(1637)
Distance from * (μm)
E
anti-NXF1
H-SET-N214(1637)

Figure 2

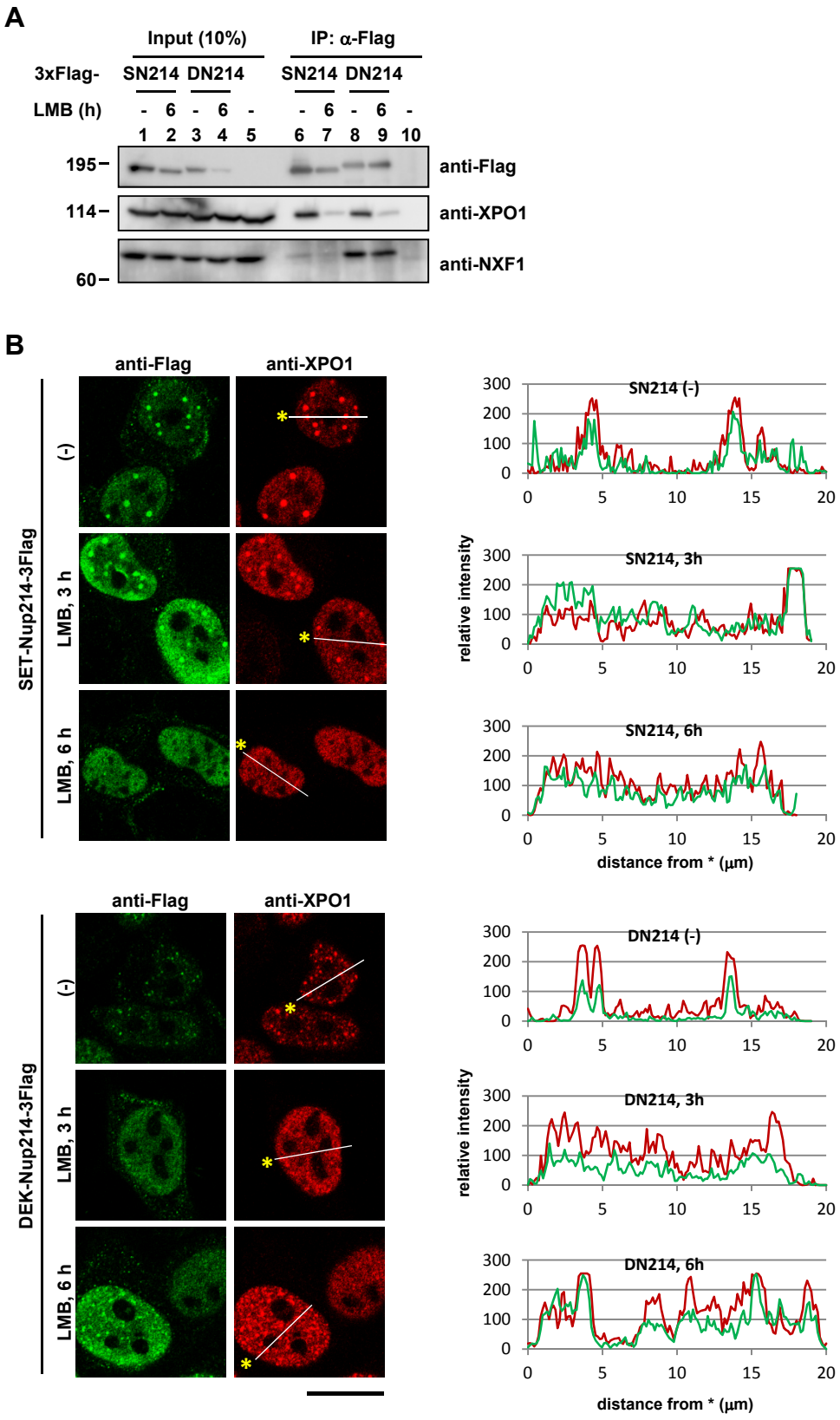
A
Input (10%)
IP: α-Flag
3xFlag-
SN214
DN214
SN214
DN214
LMB (h)
- 6 - 6 -
- 6 - 6 -
1 2 3 4 5
6 7 8 9 10
195
114
60
anti-Flag
anti-XPO1
anti-NXF1
B
anti-Flag
anti-XPO1
SET-Nup214-3Flag
(-)
LMB, 3 h
LMB, 6 h
SN214 (-)
SN214, 3h
SN214, 6h
relative intensity
distance from * (μm)
DEK-Nup214-3Flag
DN214 (-)
DN214, 3h
DN214, 6h

Figure 3

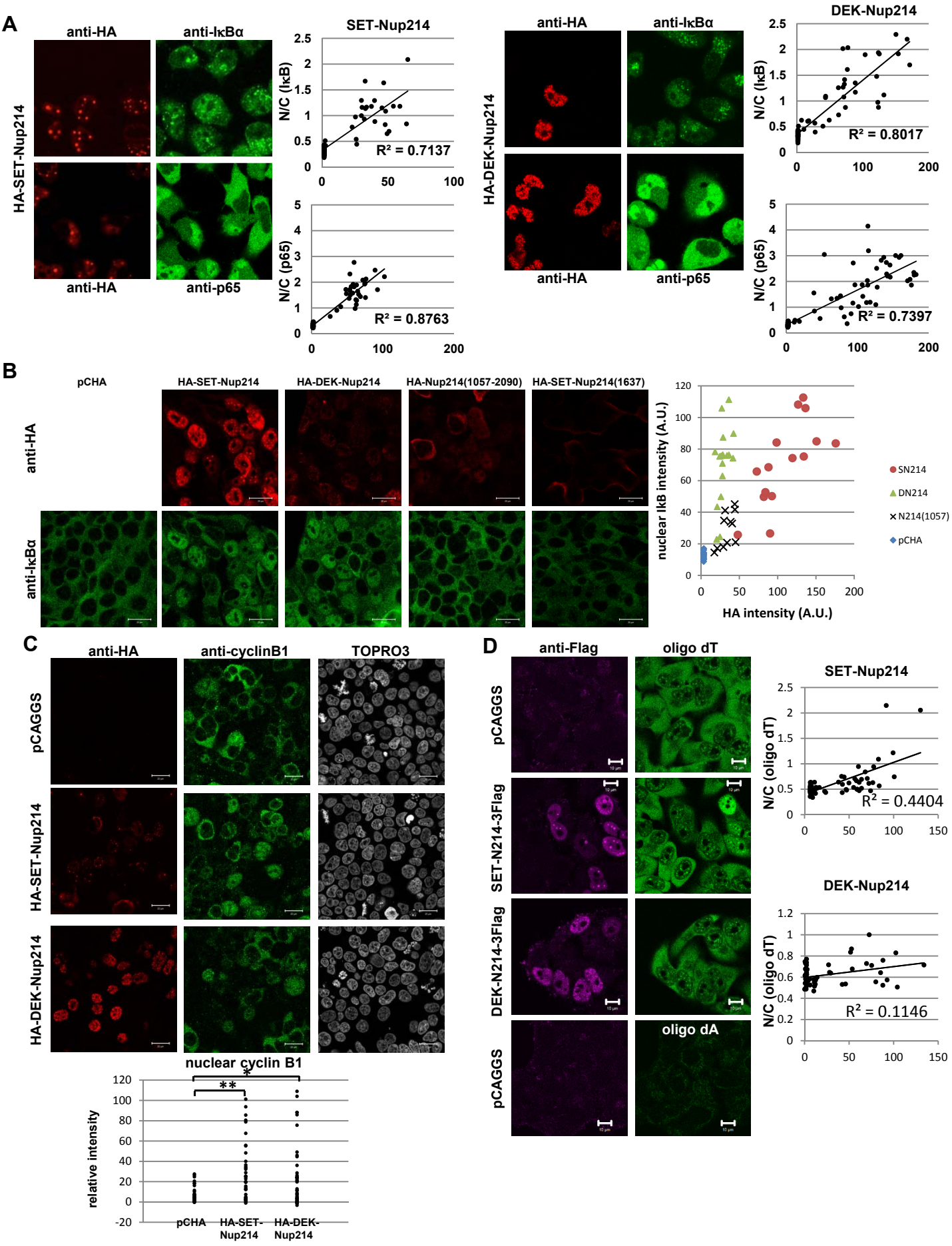
A
anti-HA
anti-IκBα
HA-SET-Nup214
anti-HA
anti-p65
SET-Nup214
N/C (IκB)
R² = 0.7137
N/C (p65)
R² = 0.8763
HA-DEK-Nup214
DEK-Nup214
R² = 0.8017
R² = 0.7397
B
pCHA
HA-SET-Nup214
HA-DEK-Nup214
HA-Nup214(1057-2090)
HA-SET-Nup214(1637)
anti-HA
anti-IκBα
nuclear IkB intensity (A.U.)
HA intensity (A.U.)
SN214
DN214
N214(1057)
pCHA
C
anti-HA
anti-cyclinB1
TOPRO3
pCAGGS
HA-SET-Nup214
HA-DEK-Nup214
nuclear cyclin B1
relative intensity
pCHA
HA-SET-Nup214
HA-DEK-Nup214
D
anti-Flag
oligo dT
pCAGGS
SET-N214-3Flag
DEK-N214-3Flag
oligo dA
SET-Nup214
N/C (oligo dT)
R² = 0.4404
DEK-Nup214
R² = 0.1146

Figure 4

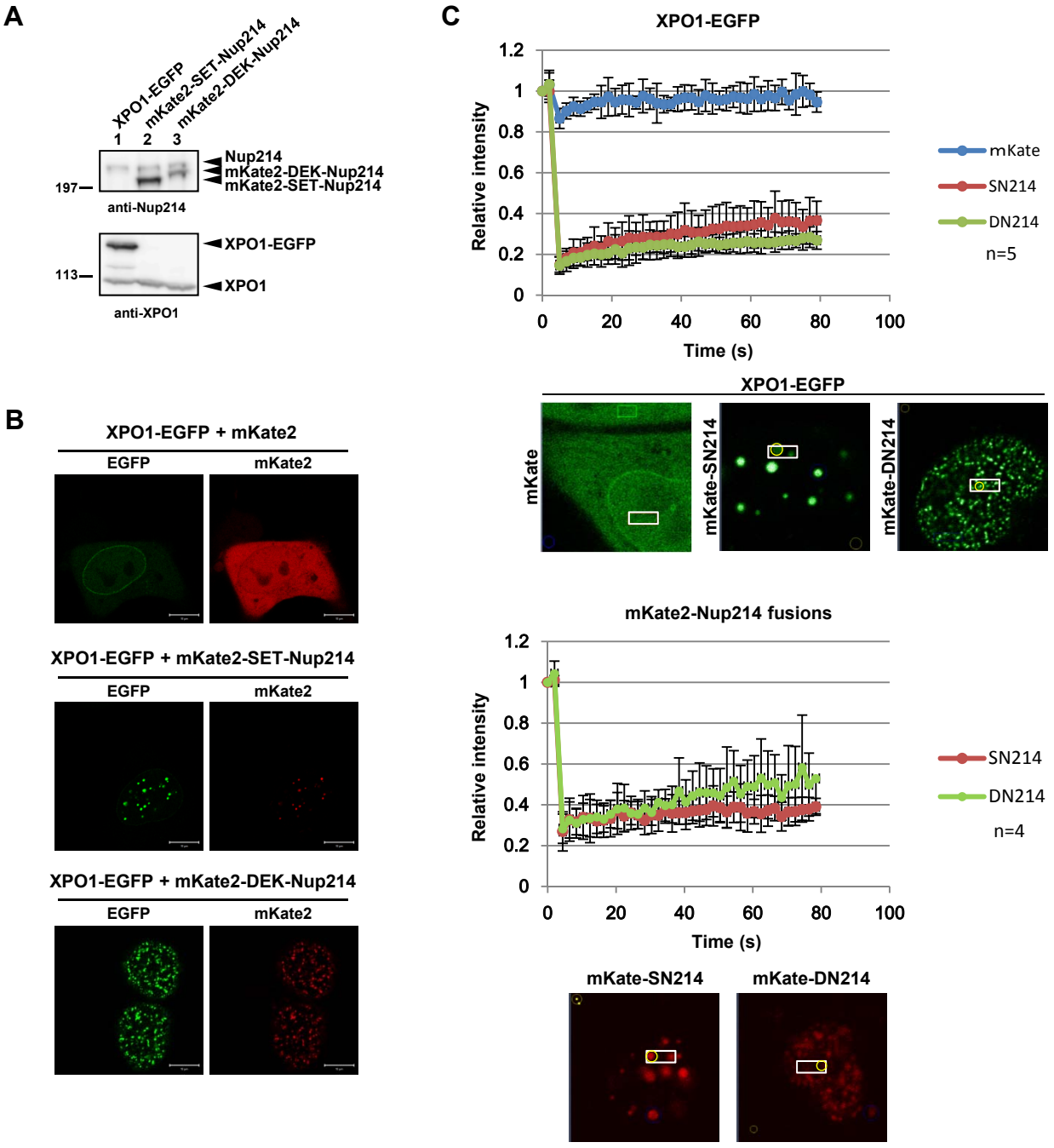
A
XPO1-EGFP
mKate2-SET-Nup214
mKate2-DEK-Nup214
1 2 3
197
Nup214
mKate2-DEK-Nup214
mKate2-SET-Nup214
anti-Nup214
113
XPO1-EGFP
XPO1
anti-XPO1
B
XPO1-EGFP + mKate2
EGFP
mKate2
XPO1-EGFP + mKate2-SET-Nup214
EGFP
mKate2
XPO1-EGFP + mKate2-DEK-Nup214
EGFP
mKate2
C
XPO1-EGFP
Relative intensity
Time (s)
mKate
SN214
DN214
n=5
XPO1-EGFP
mKate
mKate-SN214
mKate-DN214
mKate2-Nup214 fusions
Relative intensity
Time (s)
SN214
DN214
n=4
mKate-SN214
mKate-DN214

Figure 5

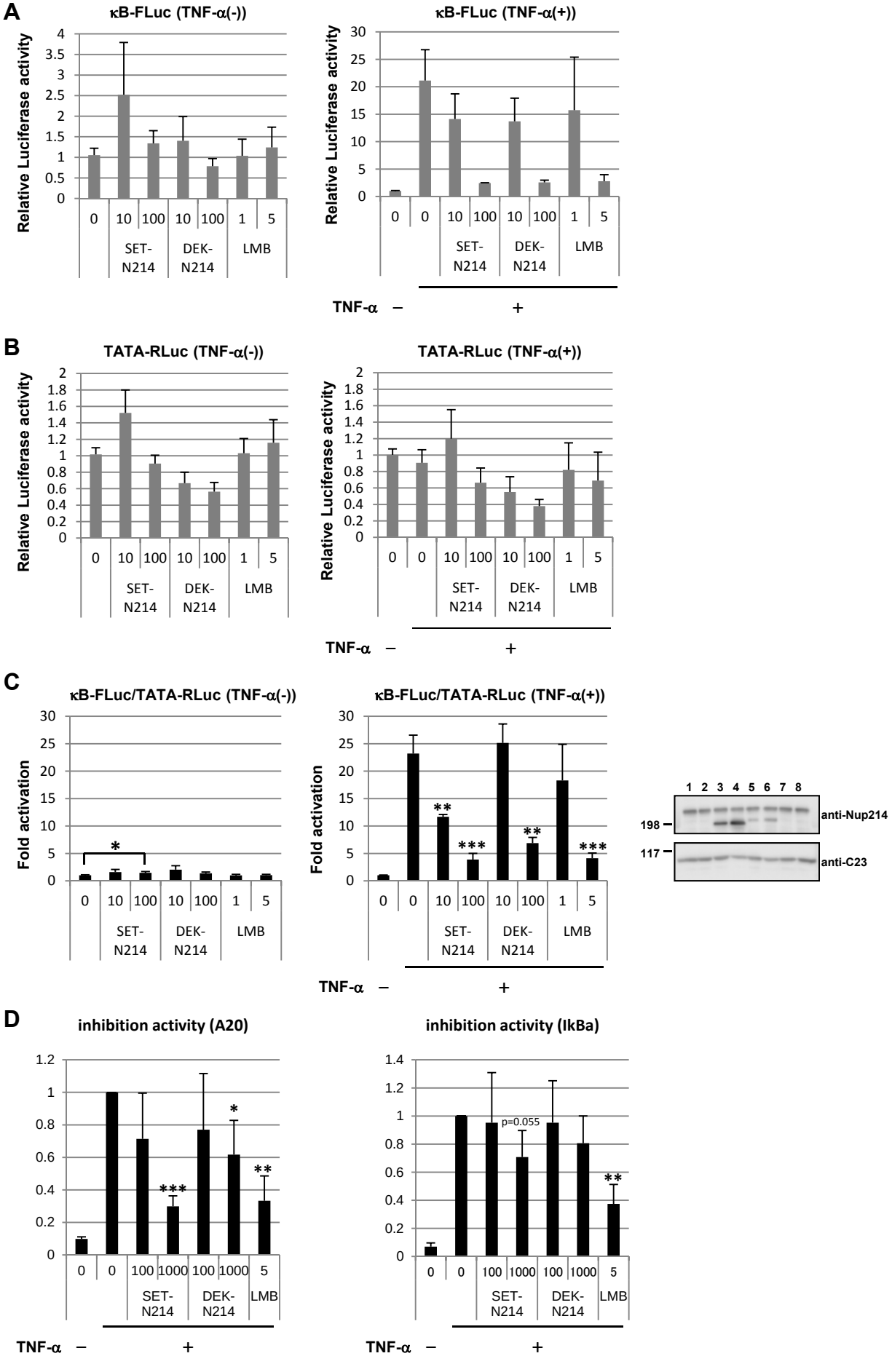
A
κB-FLuc (TNF-α(-))
κB-FLuc (TNF-α(+))
Relative Luciferase activity
0 10 100 10 100 1 5
SET-N214
DEK-N214
LMB
TNF-α – +
B
TATA-RLuc (TNF-α(-))
TATA-RLuc (TNF-α(+))
C
κB-FLuc/TATA-RLuc (TNF-α(-))
κB-FLuc/TATA-RLuc (TNF-α(+))
Fold activation
1 2 3 4 5 6 7 8
198
anti-Nup214
117
anti-C23
D
inhibition activity (A20)
inhibition activity (IkBa)
p=0.055
0 0 100 1000 100 1000 5

Figure 6

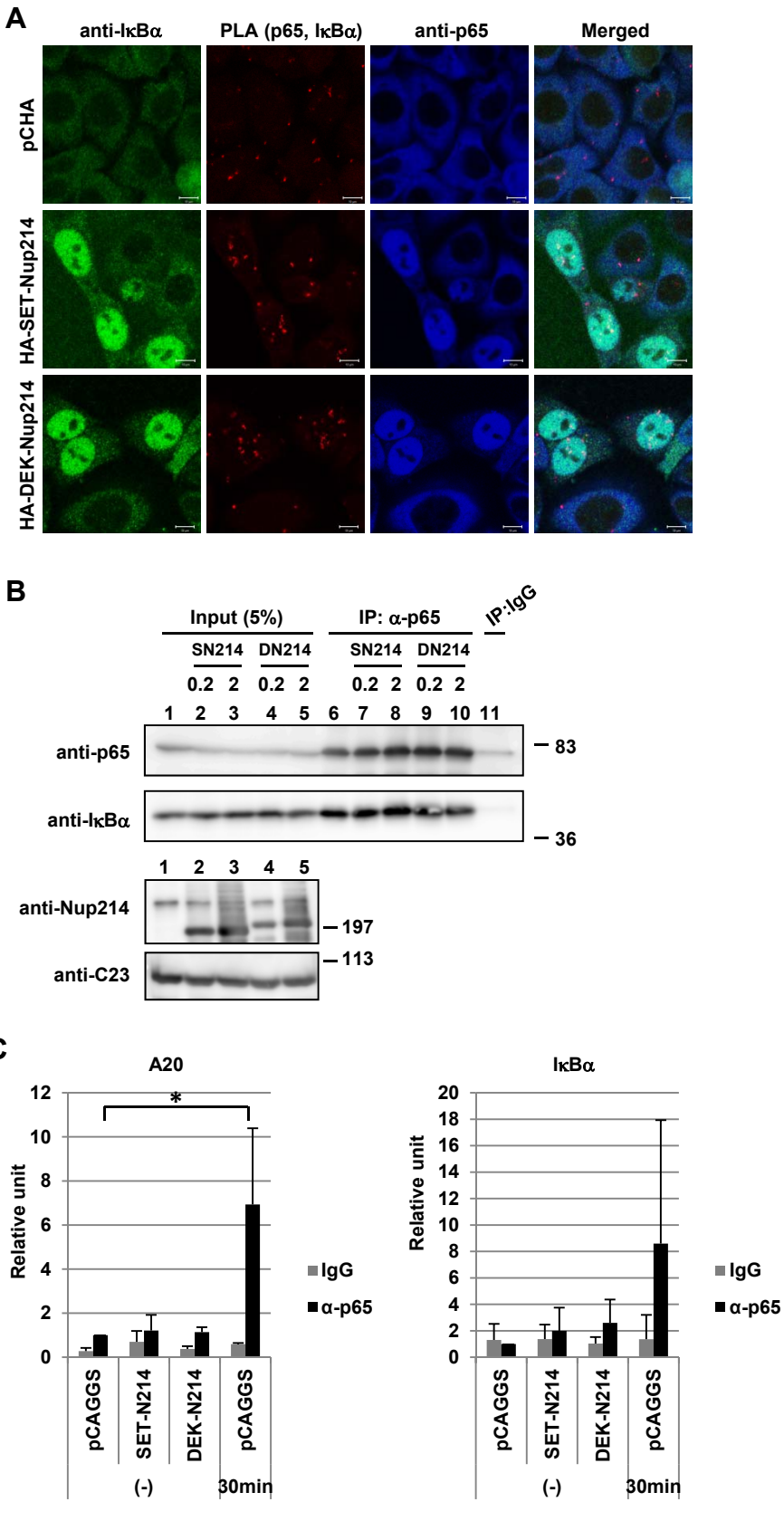
A
anti-IκBα
PLA (p65, IκBα)
anti-p65
Merged
pCHA
HA-SET-Nup214
HA-DEK-Nup214
B
Input (5%)
IP: α-p65
IP:IgG
SN214
DN214
0.2 2 0.2 2
0.2 2 0.2 2
1 2 3 4 5 6 7 8 9 10 11
anti-p65
83
anti-IκBα
36
1 2 3 4 5
anti-Nup214
197
anti-C23
113
C
A20
IκBα
Relative unit
IgG
α-p65
pCAGGS
SET-N214
DEK-N214
pCAGGS
(-)
30min

Figure 7

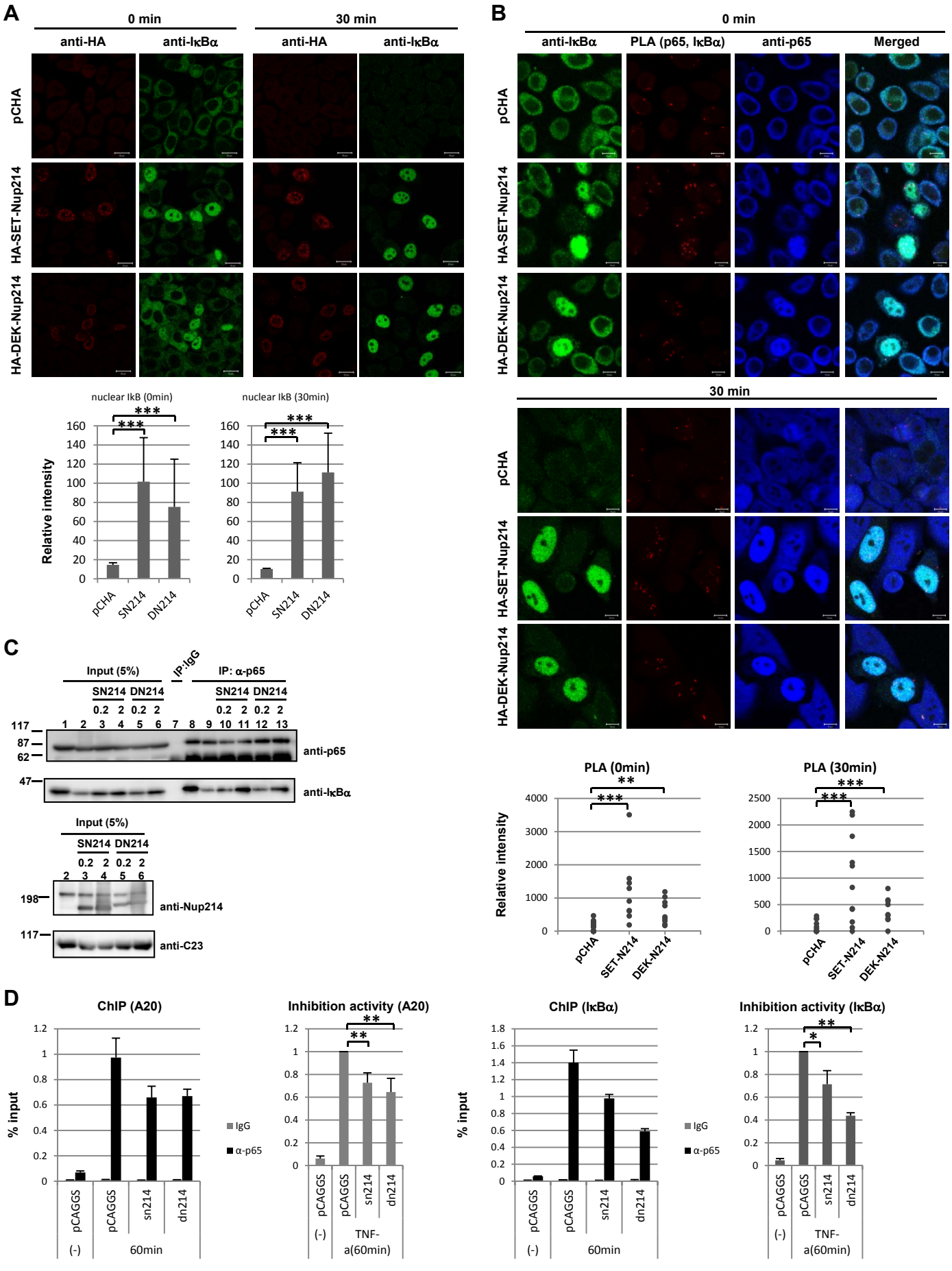
A
0 min
30 min
anti-HA
anti-IκBα
pCHA
HA-SET-Nup214
HA-DEK-Nup214
nuclear IkB (0min)
nuclear IkB (30min)
Relative intensity
pCHA
SN214
DN214
B
0 min
anti-IκBα
PLA (p65, IκBα)
anti-p65
Merged
30 min
PLA (0min)
PLA (30min)
SET-N214
DEK-N214
C
Input (5%)
IP:IgG
IP: α-p65
anti-p65
anti-IκBα
anti-Nup214
anti-C23
D
ChIP (A20)
Inhibition activity (A20)
ChIP (IκBα)
Inhibition activity (IκBα)
% input
IgG
α-p65
pCAGGS
sn214
dn214
(-)
60min
TNF-a(60min)

Figure 8

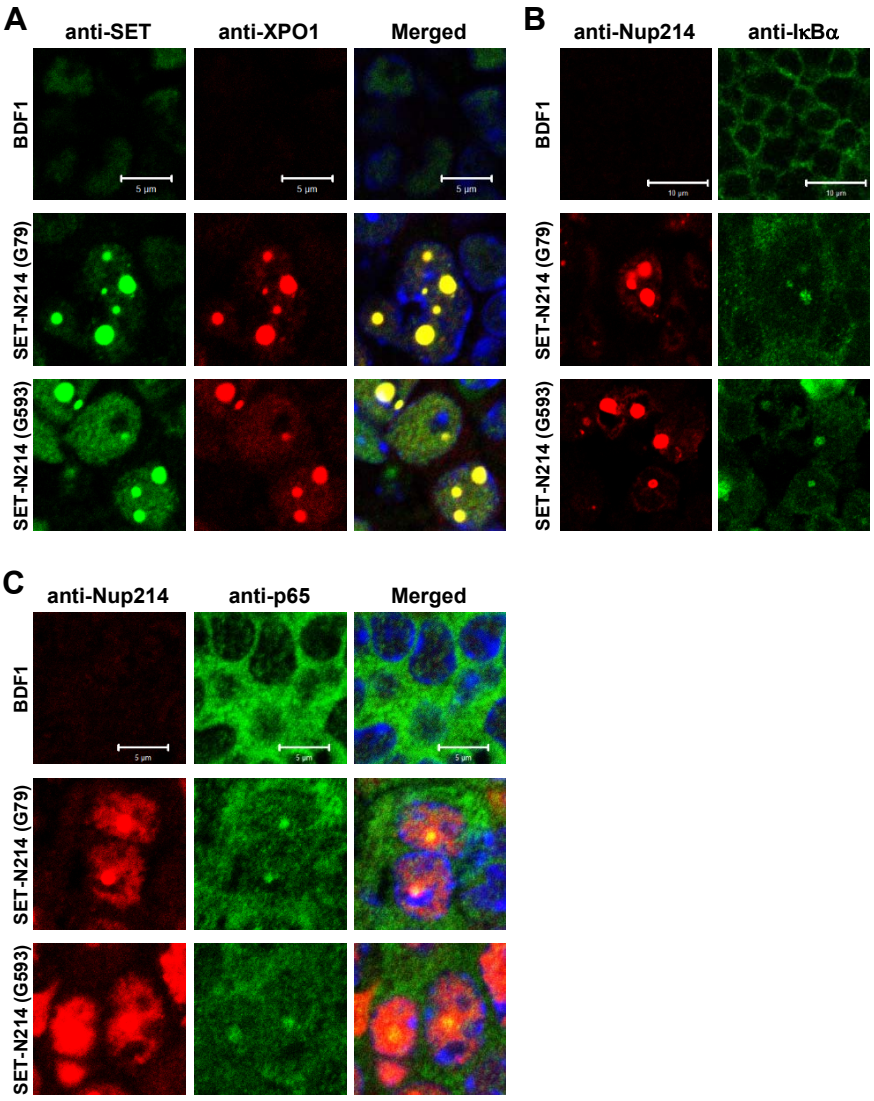
A
anti-SET
anti-XPO1
Merged
BDF1
SET-N214 (G79)
SET-N214 (G593)
B
anti-Nup214
anti-IκBα
BDF1
SET-N214 (G79)
SET-N214 (G593)
C
anti-Nup214
anti-p65
Merged
BDF1
SET-N214 (G79)
SET-N214 (G593)